USING HYSTERETIC ENERGY TO EVALUATE DAMPING CHARACTERISTICS OF HARD COATINGS ON TITANIUM

THESIS

Colin C. Engebretsen, Captain, USAF

AFIT-ENY-13-M-13

DEPARTMENT OF THE AIR FORCE
AIR UNIVERSITY

AIR FORCE INSTITUTE OF TECHNOLOGY

Wright-Patterson Air Force Base, Ohio

AFIT-ENY-13-M-13

USING HYSTERETIC ENERGY TO EVALUATE DAMPING CHARACTERISTICS OF HARD COATINGS ON TITANIUM

THESIS

Presented to the Faculty

Department of Aeronautics and Astronautics

Graduate School of Engineering and Management

Air Force Institute of Technology

Air University

Air Education and Training Command

In Partial Fulfillment of the Requirements for the

Degree of Master of Science in Aeronautical Engineering

Colin C. Engebretsen, BS

Captain, USAF

March 2013

AFIT-ENY-13-M-13

USING HYSTERETIC ENERGY TO EVALUATE DAMPING CHARACTERISTICS OF HARD COATINGS ON TITANIUM

Colin C. Engebretsen, BS
Captain, USAF

Approved:

_____	_____
Anthony N. Palazotto, PhD (Chairman)	Date
_____	_____
Richard G. Cobb, PhD (Member)	Date
_____	_____
Onome E. Scott-Emuakpor, PhD (Member)	Date

Abstract

Current methods of damping determination use half-power bandwidth or free decay methods on cantilever or free-free bending specimens under force excitation. These methods are accompanied by non-uniform bending strain evaluation; they are vulnerable to undesired air damping; and they require vibration testing equipment which is not as common in smaller labs. The measurement of hysteretic energy loss in fixed-fixed axial cyclic loading alleviates these difficulties. By using common tensile testing machines, strain is uniform and air damping is of no concern. Furthermore, the static test section allows for simplified environmental variation for high temperature or high humidity testing. This study is set forth to advance and refine the hysteretic energy method for determining material damping properties. Convergence of cyclic load rate, and data sample rate were studied to reduce extraneous system damping and relative standard deviation. Bare and hard-coated titanium bars were tested to compare coating knock-down factor to existing data from cantilever tests. Boundary conditions were studied for aluminum specimens to determine the effects of losses for different grip mechanisms, a suspected problem in previous work with this method. Peak quality factory results for 6061-T6 aluminum and Ti-6Al-4V alloys were 709 and 132 accordingly. Quality factor knockdown in titanium from the APS-600 coating was within 40% of currently published results. Threaded boundary conditions did not improve results over hydraulic grips.

I can do all things through Christ who strengthens me. Philippians 4:13

Acknowledgments

I would like to thank the fine men and women of the Turbine Engine Fatigue Facility for all their help, support, and hospitality; in particular, Dr. Scott-Emuakpor, and Dr. George for their guidance and mentorship. Above all thank you, Dr. Palazotto for your patience and encouragement, and for reminding me to always ask why.

Colin C. Engebretsen

Table of Contents

Page

List of Figures

List of Tables

Nomenclature

Symbol	Description
D_c	coating dissipated energy
D_s	system dissipated energy
D	material dissipated energy
E	elastic storage modulus
E_b	elastic storage modulus - substrate
E_c	elastic storage modulus - coating
E_l	loss modulus
E_s	elastic storage modulus – substrate/coating system
ε	strain
ε_a	strain amplitude
η	loss factor
η_c	coating loss factor
η_s	system loss factor
h	substrate thickness
K	knockdown factor
$\mu\varepsilon$	microstrain
ω	frequency
P	force
P_a	force amplitude
P_c	compressive force equation
P_t	tensile force equation
Q	quality factor
R	alternating stress or strain ratio
R-STD	relative standard deviation
σ	stress
σ_a	stress amplitude
T	period
U_c	coating stored energy
U_s	system stored energy
U	material stored energy
φ	phase angle
X	displacement
X_a	displacement amplitude
ζ	damping ratio

USING HYSTERETIC ENERGY TO EVALUATE DAMPING CHARACTERISTICS OF HARD COATINGS ON TITANIUM

I. Introduction

Research Objective

To improve turbine engine performance and decrease weight, one-piece integrally bladed disks (IBDs) have become common in modern turbomachinery (Younossi, et al. 2002). The absence of dovetail joints to provide friction damping leaves IBDs more susceptible to resonant frequency excitation and associated high cycle fatigue (HCF) failure. HCF is characterized by stresses well within the elastic limit of the material, with a high number of cycles ($>10^5$ as a rule of thumb) expected before failure (Van and Papadopoulos 1999). In turbine engines, HCF occurs at high frequencies such that a large number of cycles will inevitably accumulate between inspections (Nicholas 2006). With the friction damping of dovetail joints removed, excited IBDs are dependent on the inherent damping of the rotor material, unless additional damping material is applied.

Driven by these fatigue concerns, the characterization of damping materials has become an important area of research. Current methods of experimental damping determination are based on beam bending response at a natural frequency and use of free decay or half-power bandwidth analysis (discussed in depth later). At high frequencies and/or high strain, however, bending tests encounter significant air damping. To overcome this obstacle, vacuum chambers have been used, though they are not readily accessible. Bending tests are also constrained to fully reversed (R = -1) stress ratios. Additionally, non-uniform strain in bending makes coating property extraction difficult. The objective of this research is to investigate an alternative method through the use of

axial hysteretic energy methods for damping determination. This method would utilize common tensile test machines, and the resulting uniform strain would simplify coating property extraction. The hysteretic energy method would also open up the possibility of testing in much higher strain ranges or at stress ratios greater than fully reversed ($R > -1$). Additionally, the static test section of this method would allow simple environmental modification to include heat, humidity, or corrosive environments.

Hard Coatings

Every material exhibits inherent damping characteristics to some degree. For structural metals this internal damping can be attributed to micro structural effects such as thermal diffusion, deformation, and stress relaxation at grain boundaries; these effects, however, are typically small for most aerospace alloys (Nashif, Jones and Henderson 1985). Because the inherent damping of metallic alloys is small compared to external damping mechanisms, resonant excitation can be dissipated with the addition of damping pads or, more efficiently, by using specially designed hard coatings applied directly to the substrate material (Limarga, et al. 2007).

The study of thermal barrier coatings (TBCs) for turbine components was initiated to improve service life by means of thermal insulation and oxidation protection of substrate metals (Patsias, Tassini and Lambrinou 2006). However, these coatings were discovered to possess high damping characteristics, for which they have since been studied (Tassini, Patsias and Lambrinou 2006). Coatings such as magnesium aluminate spinel (mag spinel) and yttria stabilized zirconia (YSZ) were common subjects for damping characterization studies of late. However, these coatings were not specifically

designed for damping. Coating development has since turned toward damping optimization. The coating studied in this work is a proprietary damping treatment, referred to herein as APS-600, developed by APS Materials Inc. This coating is applied in four steps; first, a NiCrAlY bond coat is plasma-sprayed less than one mil thick; then, the desired thickness of alumina-titania ceramic is applied, also by plasma-spray; next, the coating is vacuum-infiltrated with a proprietary viscoelastic material developed by APS Materials Inc; finally, the coating is cured at 478° K for an hour. (Torvik 2012)

Damping Coating Characterization

Early tests on the damping properties of ceramic-coated specimens have been primarily vibration bending tests. Both time domain and frequency domain methods have been used to extract damping properties.

The time domain, or free-decay method, measures the decay rate for consecutive peak displacements of an unforced vibration (Reed 2007). With technology such as Laser Doppler Vibrometry (LDV), these measurements can be made quite easily. The varying strain of this test makes it ideal for measuring strain dependant damping of nonlinear materials. However, specimens with low natural frequencies, and high damping would require interpolation to extract this data. Furthermore, the test is susceptible to air damping effects, unless it is done in a vacuum, and the nature of the free-decay test also confines strain to relatively low values for coated specimens (< 1000 με) (Reed 2007).

The frequency domain method can be achieved via sine sweep or dynamic ping tests. Analysis of the frequency bandwidth over which the response amplitude is $> \frac{1}{\sqrt{2}}$

times the peak amplitude at resonant frequency can be used to determine material damping. This method again requires precise displacement measurement. Powerful electromagnetic vibration equipment allows the technique to achieve higher strains than free-decay. Unfortunately, as a linear approximation, this method will show higher than true damping for nonlinear systems, and it is still susceptible to air damping interference (Pearson 2008). The theory behind these methods will be examined further in the following chapter.

Chronological Damping Work

Vaidya tested the damping properties of plasma-sprayed alumina coated Ti-25Al-10Nb-3V-1Mo alloy. A three-point bend test was used for static property determination and piezoelectric oscillation of cantilevered beams at 100 kHz was used for damping determination. There was significantly more damping in thickly coated specimens. As a consequence, however, there was a very high vulnerability of substrate modulus to defects initiated by cracks formed in the coating. (Vaidya, et al. 1995)

Torvik's work in 2002 compared the half-power bandwidth method with the free-decay method on Hastelloy X, nickel superalloy, beams in bending. One key addition was the use of LDV to determine beam displacement without affecting the natural frequency of the specimen. An electrodynamic exciter was used for base excitation of bending specimens over a range of 5-2500 Hz. It was found that frequency response and free decay methods were shown to be in agreement and that significant differences in damping exist between modes. The achievable strain was limited by maximum equipment output force. It was also found that instrumentation precision drove a minimum amount of damping that could be measured accurately. Furthermore, it was

determined that mag spinel should provide sufficient damping to reduce vibration of blades in turbine engines. (Torvik, Patsias and Tomlinson 2002)

Ivancic studied two thicknesses of mag spinel coating on Ti-6Al-4V plates, clamped along one edge, which were vibration tested on a 26690 N shaker until failure. Failure was defined as crack propagation which directly affected resonant frequency. Dynamic ping tests were used to determine natural frequencies. Scanning laser vibrometry was used to determine plate mode shape. The half-power bandwidth method was used to determine damping properties.

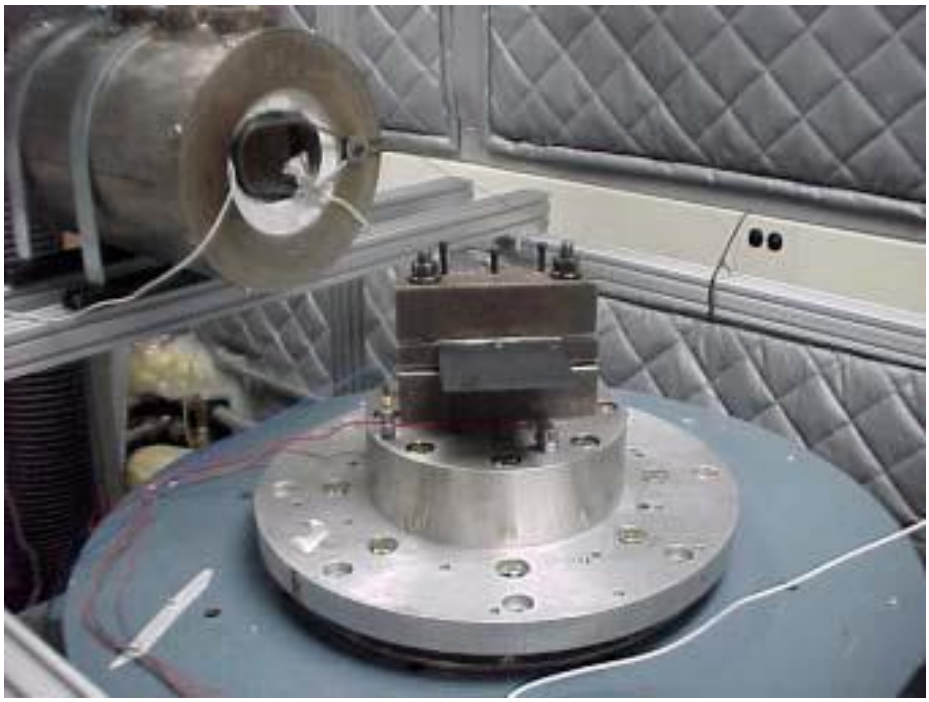

Figure 1: Test plate in 6000 lb shaker (Ivancic 2003)

Coated plates were able withstand higher substrate stress without fatigue failure. Under identical applied force, a mag spinel coated plate had a fatigue life five times that of bare plates. It was found that the thicker coatings did not dramatically improve

damping, and were susceptible to flaking at higher strain. It was also found that damping was dependent on mode shape. (Ivancic 2003)

In 2004, Patsias varied the parameters of the air plasma spraying technique in an effort to optimize damping. It was found that slightly closer than standard spraying distance and preheated substrate improved damping properties of mag spinel. Variation of spraying angle away from 90°, however, dramatically decreased damping. The work was significant in that it showed a large dependence of damping properties on the microstructure of the coating. (Patsias, Byrne and Shipton 2004)

Blackwell, like Ivancic, also used Ti-6Al-4V plates and a laser vibrometer to measure plate response to sine sweep excitation. Half-power bandwidth calculations were used to determine material damping. Plates were exposed to a relatively low 500με. It was found that damping is mode dependant in bare plates. It was also shown that mag spinel had nonlinear damping properties that were strain dependant. The damping values, however, can be expected to be higher than true due to the inaccuracies of half-power bandwidth on nonlinear systems, as previously mentioned. (Blackwell 2004)

In 2007, Reed overcame air damping effects by using electromagnets to excite a free-free Ti-6Al-4V beam in a vacuum. This study again utilized laser vibrometry as well as both free decay and half-power bandwidth methods. The free-free boundary condition was achieved by suspending beams by wires at the nodes (Figure 2). The free-free system achieved lower system damping at higher strain amplitudes due to zero losses in boundary conditions. Additionally, the vacuum environment eliminated air damping at high strain and frequency, and showed that relative damping remained constant across a broad range of strains (through 1700με).

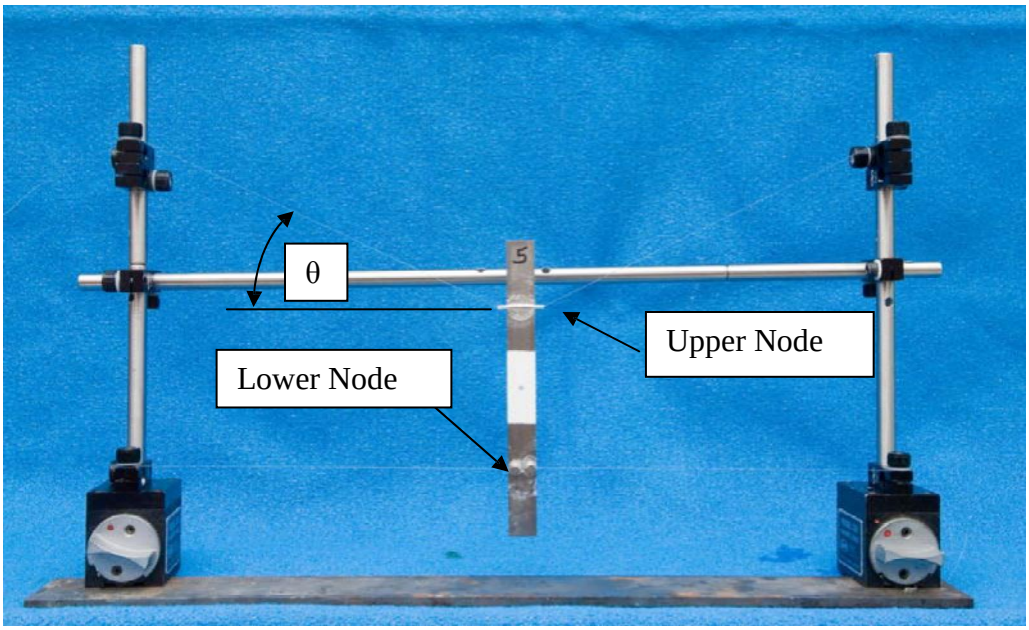

Figure 2: Free-free beam suspension system (Reed 2007)

The study also revealed the inconsistency between log decrement and half-power bandwidth results in nonlinear systems. Furthermore, it was able to identify material property changes, in mag spinel, as a result of strain history. (Reed 2007)

Research conducted by Pearson followed the same format as Reed, adding the study of YSZ. He continued the comparison of log decrement and half-power bandwidth methods on nonlinear systems, finding that variation of sine sweep rate cannot rectify the discrepancy between the two. The results also reinforced the strain history effects in mag spinel, as found by Reed. Furthermore, Pearson confirmed via scanning electron microscope that microstructural cracking of mag spinel, and YSZ coatings directly correlated to an increase in mechanical damping. (Pearson 2008)

Expanding further on the work of Reed, Easterday improved the free-free beam in vacuum chamber experimental setup with the addition of radiant heating by means of

halogen lamps. The work also looked at the contribution of the bond coat to system damping. It was found that the bond coat had negligible effect on the damping of the system. Above all, the work resulted in temperatures of up to 755° K, improving the versatility of the free-free vacuum test setup. (Easterday 2010)

Although the free-free vacuum beam method has proven to be a very effective means of measuring damping, it presents many difficulties. Logistically, specimen preparation for free-free testing is very delicate and time consuming processes. Furthermore, the equipment to conduct the test (vacuum chamber, electromagnets, & radiant heaters) is very specialized and not readily available in every material lab. Radiant heat, moreover, requires exacting equations to accurately reach desired temperatures. In addition, the mathematical methods for extracting properties from bending tests, in general, are complex due to non-uniform strain throughout the specimen. Standard shaker and free decay tests must account for air damping, and vibration equipment is not always available in smaller lab facilities. Alleviation of these complexities has been under investigation by means of hysteretic energy methods in cyclic axial loading. Initial test have shown reasonable repeatability of damping measurements in 6061-T6 Aluminum specimens, albeit with larger than expected dissipated energy as a possible consequence of boundary condition losses at the gripping mechanism used for the study (Scott-Emuakpor, Runyon and George 2012).

Hysteresis Method

The hysteretic energy method of damping determination is studied in this work. Due to very subtle inelasticity under different loading conditions, structural materials

under sinusoidal load cycles exhibit load-deformation curves that do not form a straight line, but instead generate a hysteresis loop proportional to the dissipated (damped) energy (Lazan 1968).

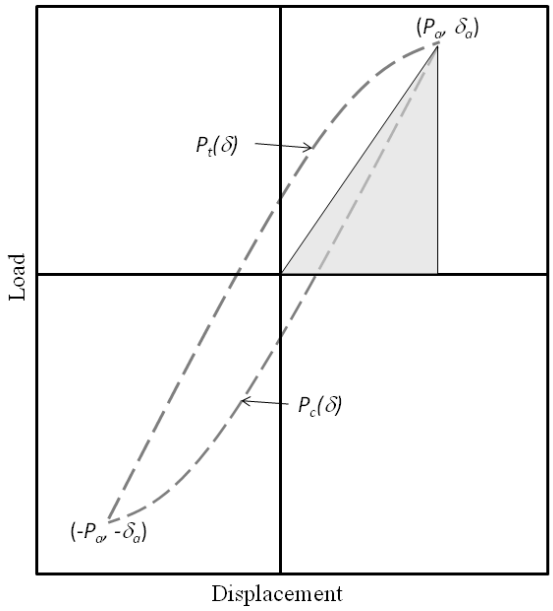

Figure 3: Hysteresis loop diagram (Scott-Emuakpor, Runyon and George 2012)

Because inherent damping in metallic materials is quite small, the resultant hysteresis loop requires very precise measurements to detect. This explains why evaluation of hysteresis energy to determine material damping has not been highly utilized to date. The use of longer specimens will result in larger and, thus, more measurable displacement for a given strain. Measurement of displacement via linear variable differential transformer (LVDT) has become increasingly accurate of late. Add to that the prevalence of computing programs such as MATLAB to eliminate graphical "square-counting" for hysteresis area measurement. Technology has brought the feasibility of the hysteretic energy method within reach.

Intent of Research

The intent of this research is to continue the investigation and refinement of the axial hysteretic energy method as a means for damping characterization. This method utilizes commonplace tensile testing machines, resulting in uniform strain and simplified mathematics compared to bending techniques. It alleviates any concern of air damping and makes environmental modification simple due to the static accessibility of the specimen test section. Furthermore, hysteretic methods open damping tests to the possibility of stress ratios outside of the fully reversed (R = -1) norm that is requisite in vibratory beam bending tests (Scott-Emuakpor, Runyon and George 2012). Six primary studies are set forth to advance damping determination by means of the hysteretic energy method.

1. Replicate 6061-T6 Aluminum test results on MTS tension test machine with more precise computer controller & data logging.
2. Investigate boundary condition effects by testing directly threaded specimens to compare to mechanically gripped specimens.
3. Conduct high stiffness compliance tests to quantify energy dissipation in the mechanically gripped boundary conditions.
4. Conduct convergence studies to determine optimal cyclic load rates and data sample rates to achieve the most precise measure of material damping.
5. Conduct hysteretic damping tests on Ti-6Al-4V titanium specimens to compare to readily available damping properties of bending methods.
6. Use hysteretic damping tests to compare damping reduction of APS-600 on Ti-6Al-4V to results obtained from bending tests.

Overview

The following chapters will first develop the theory behind the hysteretic energy method. Next, the experimental process used herein will be examined in detail. Then, a discussion of the results obtain will follow. Finally some meaningful conclusions will be made, and the future research will be drawn out from these conclusions.

II. Theory

Objective

The objective of this section is to develop the necessary equations to characterize material damping. First, the hysteretic energy method will be developed for use in this study. Then, an understanding of current time domain and frequency domain methods will be established for comparison. Finally, a coating property extraction theory will be established.

Hysteretic Damping

Hysteretic damping is the dissipation of energy from a system acted upon by a sinusoidal forcing function

$$P(t) = P_a \sin(\omega t) \tag{1}$$

(Lazan 1968)

where

P = Instantaneous force (N)
P_a *= Force amplitude* (N)
ω *= Frequency* (rad/s)
t = Time (s)

For loads in the elastic region of a structural alloy, the system can be assumed to be linear; for which the displacement response can then be characterized as:

$$X(t) = X_a \sin(\omega t - \varphi) \tag{2}$$

(Torvik 2013)

where

X = *Instantaneous displacement* (m)
X_a = *Displacement amplitude* (m)
φ = *Phase lag* (rad)

The *period* over which one cycle occurs, T (s), can then be determined by dividing the radians per cycle (2π) by the frequency of the function arriving at:

$$T = \frac{2\pi}{\omega} \tag{3}$$

(Meirovitch 2001)

The work done per cycle can then be determined by the integral over that cycle:

$$D_s = \int_0^{\frac{2\pi}{\omega}} P(t)\left(\frac{dX}{dt}\right) dt \tag{4}$$

where D_s represents the *system dissipated energy* (J), then substituting in equation (1) and the derivative of equation (2):

$$D_s = \int_0^{\frac{2\pi}{\omega}} [P_a \sin(\omega t)]\,[\omega X_a \cos(\omega t - \varphi)]\, dt \tag{5}$$

which reduces to

$$D_s = \pi X_a P_a \sin(\varphi) \tag{6}$$

(Nashif, Jones and Henderson 1985)

Next, it is advantageous to calculate the maximum stored energy of the linear system which is defined to be half the product of the peak displacement and corresponding peak force, a point which occurs 1/4 of the way through the cycle, or at the

point where $\omega t - \varphi = \frac{\pi}{2}$. Substituting this into equations (1) & (2) the peak displacement is then established as

$$X_{max} = X_a sin\left(\frac{\pi}{2}\right) \tag{7}$$

and corresponding peak load is

$$P_{max} = P_a sin\left(\frac{\pi}{2} + \varphi\right) \tag{8}$$

Then taking one half the product of these obtains

$$U_s = \left(\frac{1}{2}\right)\left[X_a sin\left(\frac{\pi}{2}\right)\right]\left[P_a sin\left(\frac{\pi}{2} + \varphi\right)\right] \tag{9}$$

where U_s represents *system strain energy* (J), which then reduces to

$$U_s = \left(\frac{1}{2}\right) P_a X_a \cos(\varphi) \tag{10}$$

then, dividing (10) into (6):

$$\frac{D_s}{U_s} = 2\pi \tan(\varphi) \tag{11}$$

Last, divide thru by 2π to define the basic measure of hysteretic damping:

$$\eta_s = \frac{D_s}{2\pi U_s} = \tan(\varphi) \tag{12}$$

where η_s is the *system loss factor* and is unitless. (Nashif, Jones and Henderson 1985)

The inverse of loss factor is also commonly referenced:

$$Q_s = \frac{1}{\eta_s} = \frac{2\pi U_s}{D_s} = \frac{1}{\tan(\varphi)} \tag{13}$$

where Q_s is the *system quality factor*, which is also unitless. (Meirovitch 2001)

It should be noted that calculating loss factor from the tangent of phase lag hinges on the assumption of a linear system. Nonlinear systems are quite common, particularly when dealing with very high strain ranges in metallic alloys, or when studying viscoelastic materials. In such cases η_s and Q_s can still be accurately determined using measured dissipated and peak stored energy.

This approach is based on overall force and displacement measurements of an experimental system, and is independent of material geometry. However, any experimental system will also include dissipated energy that occurs at the boundary conditions and into the surrounding environment. The resultant system loss factor can then be broken down to account for the dissipated energy of each part of the system:

$$\eta_s = \frac{D_{coating} + D_{substrate} + D_{grips} + D_{environment}}{2\pi U_s} \quad \textbf{(14)}$$

(Torvik 2011)

This complexity can be bypassed by using stress and strain measurements to determine energy per unit volume as follows:

$$D = \int_0^{\frac{2\pi}{\omega}} \sigma \left(\frac{d\varepsilon}{dt}\right) dt \quad \textbf{(15)}$$

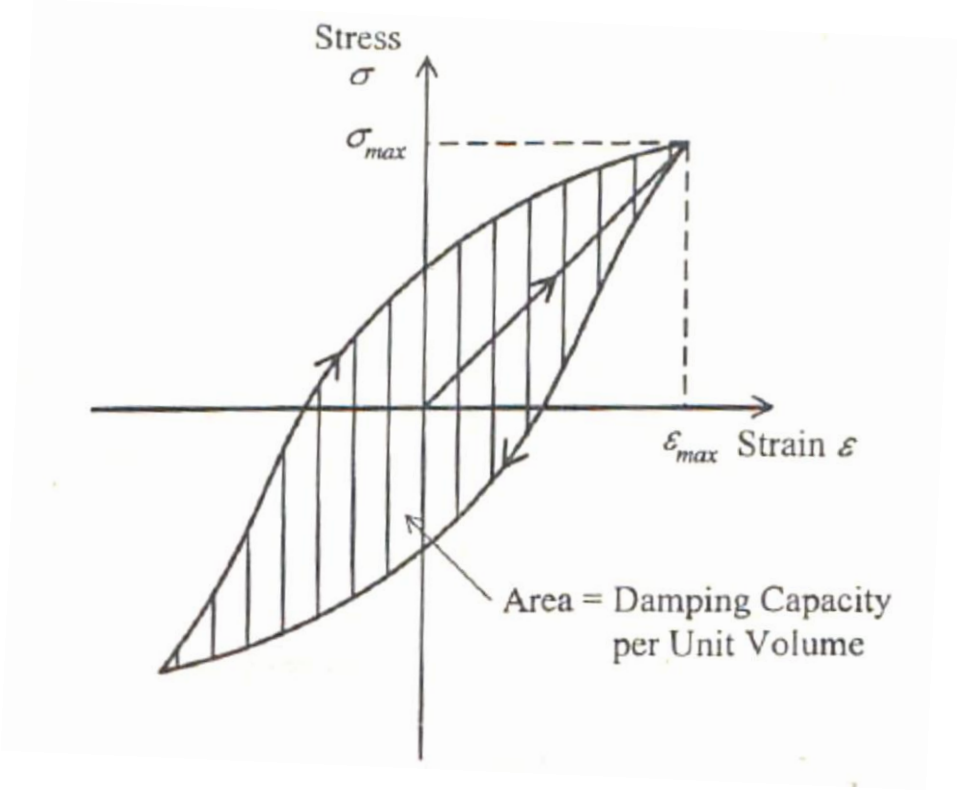

Figure 4: Stress-Strain Hysteresis (Indian Institute of Technology Roorkee)

where

D = material dissipated energy per unit volume (J/m^3)
σ = stress (Pa)
ε = strain (m/m)

then

$$U = \left(\frac{1}{2}\right)\sigma_{max}\varepsilon_{max} \tag{16}$$

where

U = material strain energy per unit volume (J/m^3) at maximum stress and strain.

Equations (15) and (16) then bring about

$$\eta = \frac{D}{2\pi U} \tag{17}$$

where

η = *material loss factor* (unitless)

This measure of damping is for the material only. In a perfect experimental system, where no energy is dissipated by the boundary conditions, or environment, the system loss factor would be equal to the material loss factor ($\eta = \eta_s$). In practical tests, however, this is not possible. Direct measurement of strain would yield the most accurate damping properties for the test material. Due to extensometer slipping, however, these results were not reliable in this study.

Current Method Comparison

Current methods of material damping determination are based on the assumption that the linear system can be directly compared to viscous damping terms. The *viscous damping ratio, ζ,* relates directly to loss factor by the equation $\eta = 2\zeta$. Two common techniques are prominent, working in both the time domain and frequency domain of a bending beam system.

Time Domain

The time domain method plots the free decay of a beam set in motion with an initial position. The displacement of the end of the beam is characterized by the equation:

$$x(t) = x_0 e^{-\zeta\omega t}\cos(\omega_d t) \tag{18}$$

where

x_0 = *Initial displacement* (m)
ζ = *Damping ratio* (unitless)
ω = *Undamped natural frequency* (rad/s)
ω_d = *Damped natural frequency* (rad/s)

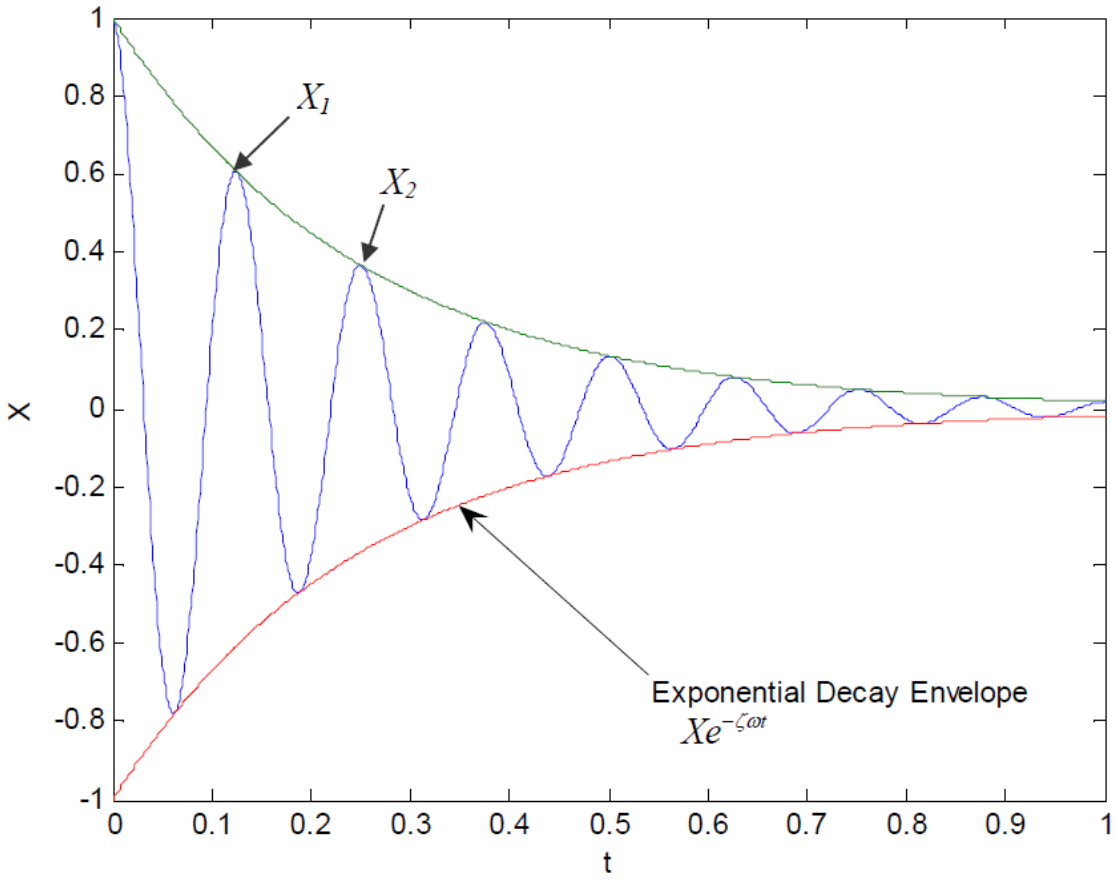

Figure 5: Time domain free decay damping (Reed 2007)

The free decay of the system can then be determined by observing the amplitudes (X_1 and X_2) of successive peaks at times t and $t+T$ as noted in Figure 5 (note that $cos(\omega_d t)$ will be equal to one at peak amplitudes):

$$X_1 = x_0 e^{-\zeta\omega t} \tag{19}$$

$$X_2 = x_0 e^{-\zeta\omega(t+T)} \tag{20}$$

where the period, T is now defined in terms of the damped natural frequency: $T = 2\pi/\omega_d$. The natural log of the ratio of these peaks is then taken:

$$\ln\left(\frac{X_1}{X_2}\right) = \ln\left(\frac{x_0 e^{-\zeta\omega t}}{x_0 e^{-\zeta\omega(t+T)}}\right) = \zeta\omega T \tag{21}$$

Thus, the damping ratio can then be found entirely from empirically measured values as seen in Figure 5:

$$\zeta = \left(\frac{1}{\omega T}\right) ln\left(\frac{X_1}{X_2}\right) \tag{22}$$

(Reed 2007)

Frequency Domain

The frequency domain, or half-power bandwidth, method is conducted via base excitation of a beam over a broad frequency sweep. This empirical approximation involves the measurement of the system response, X_{max}, at the natural frequency, ω.

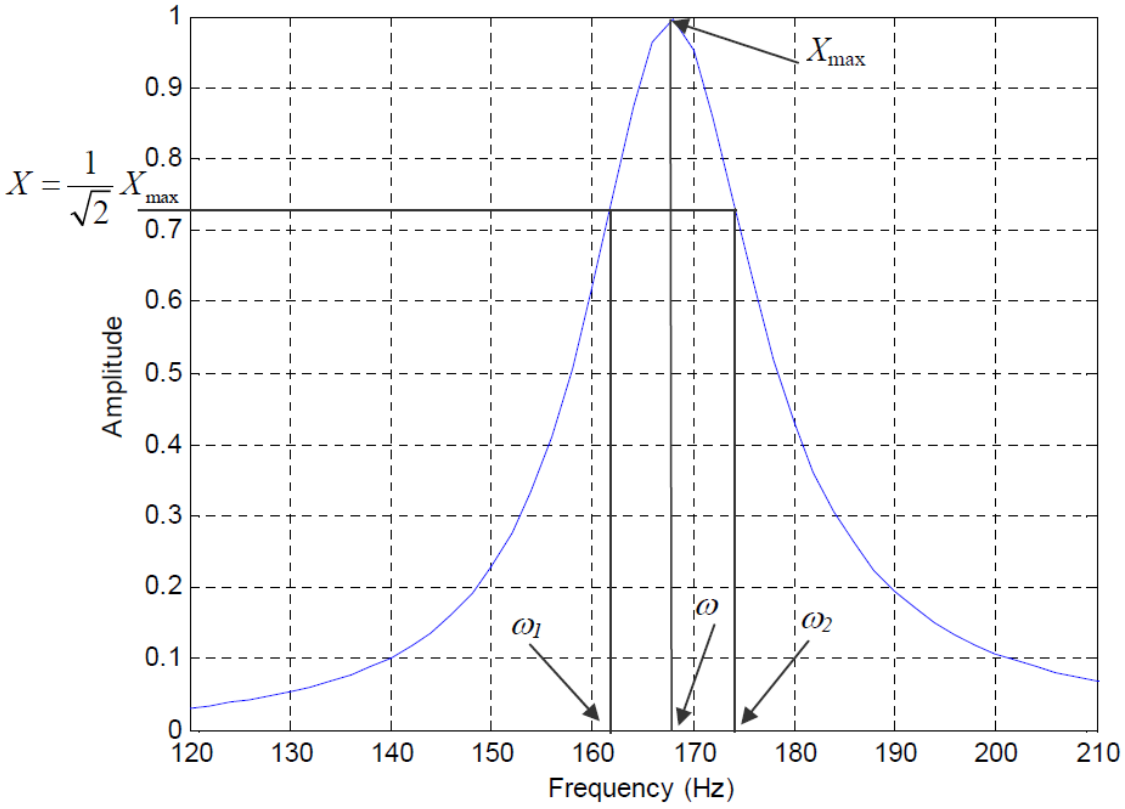

Figure 6: Half-power bandwidth approximation (Reed 2007)

Then a measurement of frequencies ω_2 and ω_1, above and below natural frequency ω, corresponding to amplitudes $X = \frac{1}{\sqrt{2}} X_{max}$ (Figure 6). From these values it can be shown that:

$$\zeta = \frac{\omega_2 - \omega_1}{2\omega} \tag{23}$$

Though effective for most aerospace alloys, the half-power bandwidth method has been shown to provide higher than true damping values for nonlinear systems. (Reed 2007)

As mentioned, both of the methods utilize viscous methods for structural damping at a natural frequency. The hysteretic method will use frequencies far below the natural

frequency of the specimen. Furthermore, the bending cases observe entirely different mode shapes than axial analyses. As a result, material damping values in bending versus axial methods will not be directly compared. With the addition of a hard coating, however, the ratio of quality factors before and after coating application will still serve as a viable comparison. The examination of coating property extraction will thus be required.

Coating Property Extraction

With suitable damping characterization established, interest is drawn to the determination of hard coating effects on damping. Ceramic coatings, such as APS-600, cannot be formed into a solid specimen due to inadequate manufacturing processes. This means that they must be bonded to a metallic substrate, such as Ti-6Al-4V, for testing and property extraction. First, the method of mixtures is used for static analysis:

$$E_s = \frac{V_c}{V_s} E_c + \frac{V_b}{V_s} E_b \tag{24}$$

where

E_s = *Elastic modulus of the substrate/coating system* (Pa)
E_c = *Elastic modulus of the coating* (Pa)
E_b = *Elastic modulus of the substrate* (Pa)
V_s = *Volume of the substrate/coating system* (m^3)
V_b = *Volume of the substrate* (m^3)
V_c = *Volume of the coating* (m^3)

Substrate volume and modulus are easily measured before the coating is applied. After coating, the system volume and modulus are easily measured. Equation (24) can then be used to solve for coating modulus resulting in:

$$E_c = \left(\frac{V_s}{V_c}\right) E_s - \left(\frac{V_b}{V_c}\right) E_b$$

(25)

Since maximum strain is constant throughout the system, (25) can be combined with Hooke's Law, $\sigma_c = E_c \varepsilon$ put into equation (16) and multiply by V_c to arrive at:

$$U_c = \left(\frac{1}{2}\right) E_c \varepsilon_a^2 V_c$$

(26)

(Nashif, Jones and Henderson 1985)

where U_c is the *peak energy stored in the coating* (J).

Next, the comparison of two different systems can be accomplished; noting from equation (14) the dissipated energy of the system before the coating is applied:

$$D_{s\,(uncoated)} = D_{substrate} + D_{grips} + D_{environment}$$

(27)

with all else left the same after the coating is applied, the dissipated energy of the system after application becomes:

$$D_{s\,(coated)} = D_{coating} + D_{substrate} + D_{grips} + D_{environment}$$

(28)

The dissipated energy of the coating can then be extracted:

$$D_c = D_{s\,(coated)} - D_{s\,(uncoated)}$$

(29)

Finally, equations (26) and (29) can be used to find the *coating loss factor* (η_c):

$$\eta_c = \frac{D_c}{2\pi U_c}$$

(30)

While the direct characterization of coating properties is important, the dependence on coating modulus adds a step. To avoid volumetric calculations for specimens with complex geometry, it is also advantageous to quantify the effect a coating

has on the damping of the structural member being studied. This is done by taking the ratio of quality factors before and after coating to get a term referred to as *knockdown factor* (K) which is unitless:

$$K = \frac{Q_{substrate}}{Q_{substrate+coating}} \quad \textbf{(31)}$$

Knockdown factor is still dependent on substrate to coating volume ratio, but for coated specimens with equivalent volume ratios the ease of comparison is significant.

The knockdown factor for a bending based test should not be directly compared to the knockdown factor for the hysteretic energy method. For a given peak stress, the stress in the axial specimen will be entirely uniform throughout the cross-section. For the same peak stress, the stress varies linearly through the cross-section (Figure 7).

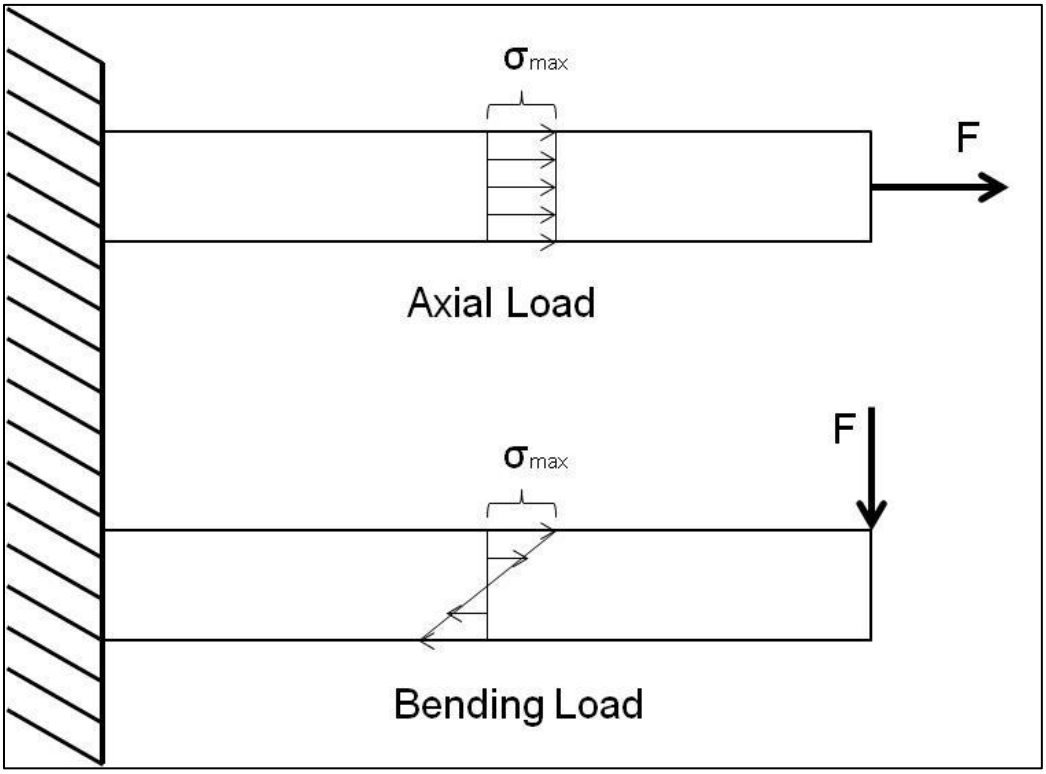

Figure 7: Bending vs. Axial Stress distribution

In both cases, however, the coating will also carry the maximum stress. As a result, we observe the average stress ratios in each case compare by the following equation:

$$\frac{1}{3} * \left(\frac{\sigma_{coating}}{\sigma_{substrate}}\right)_{bending} = \left(\frac{\sigma_{coating}}{\sigma_{substrate}}\right)_{axial} = 1 \quad \textbf{(32)}$$

The coating applied to the bending specimen, therefore, will more easily damp vibration that the coating applied to the axial specimen. To compare knockdown factors between the two cases, the knockdown factor of the axial case will be multiplied by three to relate more closely to the higher knockdown factor in the bending case.

Summary

This chapter developed the equations required to determine damping properties and compare them to current methods. Furthermore, the technique of coating property extraction and knockdown factor was established to allow comparison to current data. Next, the experimental setup will be examined.

III. Experimental Setup

General Setup

All experiments were conducted on an MTS 312 Tensile Test Machine controlled by a Flex Test 60 load frame controller, and MTS 793 station manager control software. An MTS 647.10A side-loading hydraulic wedge grip system with MTS 685 hydraulic grip supply was used for the majority of the tests, with the exception of the boundary condition study, in which these grips were removed to allow a directly threaded specimen for comparison. Loads were measured by an MTS 661, 88,964 N load cell, and displacement was measured by an MTS 204 LVDT. Strain measurements were taken with an MTS 634.12E-24 extensometer, with 25.4 mm gauge length, placed in the middle of the specimen test section. Calibrations of the load cell, LVDT, and extensometer all indicated less than 0.3% error across the range of loads and displacements seen in this study. It was found, however, after the completion of this study that an erroneous calibration caused the load cell to indicate loads 12.4% higher than actual. All data within has been adjusted for this error unless otherwise indicated. Prior to each test, the wedge grips were aligned by clamping a designated alignment plate, bringing the lower, free-rotating actuator and grip in line with the fixed upper grip (

Figure 8). This alignment ensured that no torsion was applied to the specimen.

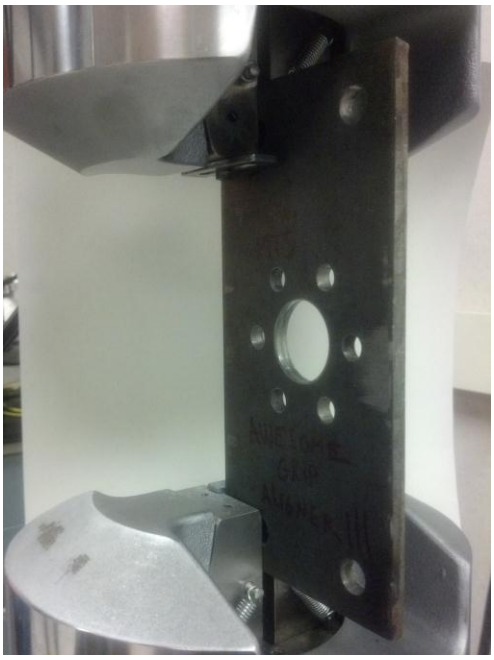

Figure 8: Alignment Plate in Hydraulic Grip Fixture

Three specimens were studied for this research. Square and round aluminum specimens were studied. The specimens were designed to a length long enough to reduce uncertainty in displacement measurements but not so long as to buckle under compression. Cyclic load amplitudes were chosen to achieve approximately 1400-1500 με – enough to provide ample hysteresis and compare to the strain ranges of published damping data.

Each specimen was subjected to a 4000 cycle break-in test, to identify the number of cycles necessary to stabilize any shifting boundary conditions and settling material properties. It was determined that the 4000 cycle break in served to adequately settle any variation in damping properties. Boundary conditions appeared to settle after only 200 cycles. With this information, the tests were set at 500 cycles; the first 200 cycles served to settle boundary conditions and were ignored, the subsequent 300 cycles to be useable

data from which to extract damping properties. This procedure was in keeping with that of Scott-Emuakpor et al., and was used for all test specimens in this work. The average of 300 cycles was used to overcome inherent instrumentation noise and data acquisition uncertainty.

Because the hydraulic grip system is not perfectly rigid, there will inevitably be some deformation, called compliance, during cyclic loading (Instron Corporation 2006). This compliance was measured by inserting a plate of AISI 4140 steel, with larger cross-sectional area than that of specimen considered for testing (Figure 9). The displacement of this steel could be assumed as very nearly zero at the loads applied for hysteresis tests. Dissipated energy from this test could be attributed entirely to the grip, and subtracted from hysteresis tests to provide more accurate substrate damping measurements.

Figure 9: Compliance Test on AISI 4140 Steel Plate

Convergence Studies

In order to accurately extract the damping properties of coatings, the extraneous damping in the test apparatus must be quite low (i.e. higher measured values of Q). For every change in specimen material or boundary conditions two convergence studies were conducted to achieve the highest Q with the lowest relative standard deviation (R-STD) between cycles. The first study varied the frequency of the cyclic load from 0.2 Hz to 3.0 Hz. For this study, the data sample rate was varied such that approximately 128 data points were collected per cycle. A forcing frequency of 1 Hz provided the highest measured Q values, thus minimal extraneous damping in test apparatus. At this cyclic load frequency, the data sample rate was varied from 128 Hz to 1024 Hz to reduce the R-STD across the 300 measured hysteresis loops in each test. These two tests were repeated for every change of specimen material or boundary condition.

Replication of Past Results in Aluminum

The first phase of the study was to improve upon the published results of hysteretic damping in 6061-T6 aluminum bar stock (Scott-Emuakpor, Runyon and George 2012), which was chosen for its low cost and inherently low damping properties. The same 6.35 x 6.35 mm square specimens were reused for this study on the same equipment, improved by recently upgraded controller and software. Each specimen was 228.3 mm long, with 57.15 mm to be gripped on either side, leaving a 114.3 mm working test section.

Figure 10: V-notch Wedges

To eliminate the possibility of bending loads, a V-notch wedge grip was used to grip the square specimen at a 45° angle centered on the load path (Figure 10). A cyclic load of 3752 N was applied at 0.2 Hz, to match the original study, achieving strains of approximately 1500 με. With these parameters fixed, the data sample rate was varied to determine how much improvement could be achieved by collecting more data points per cycle. With a proper representation of how much improvement was gained with the new controller and software, the aforementioned convergence studies were then conducted to optimize the test parameters for the square aluminum stock. The improved controller did show better R-STD values within tests. Convergence studies showed the highest Q values of 435 at 1 Hz cyclic load rate, and showed little improvement in data accuracy above a sample rate of 409 Hz.

The grip compliance test with AISI 4140 steel under these test parameters provided inaccurate results for energy dissipated at the grip. The loads used on the

square aluminum bar seemed to be too small to cause accurately measurable compliance in the system. Therefore, no additional dissipated energy was subtracted from the test measurements.

Boundary Condition Study

To eliminate the damping effects of the hydraulic wedge grip system, a more fixed boundary condition was achieved by directly threading specimens into the load cell and hydraulic actuator and securing them with locknuts. Round 6061-T6 aluminum bar stock (25.4 mm diameter) was used for ease of manufacturing threaded ends (UNF 1-14) to fit the test equipment. Each specimen was 228.6 mm long, with 57.15 mm to be threaded at the ends, leaving a 114.3 mm working test section between lock nuts. To again achieve 1500 με, a cyclic load of 47490 N was used. To eliminate misalignment between the actuator and the load cell, the first threaded specimen was affixed with strain gauges on the bottom, middle, and top of the test section, at 90° separation, a total of twelve gauges (Figure 11). Strain readings were run through an MTS 709 alignment system.

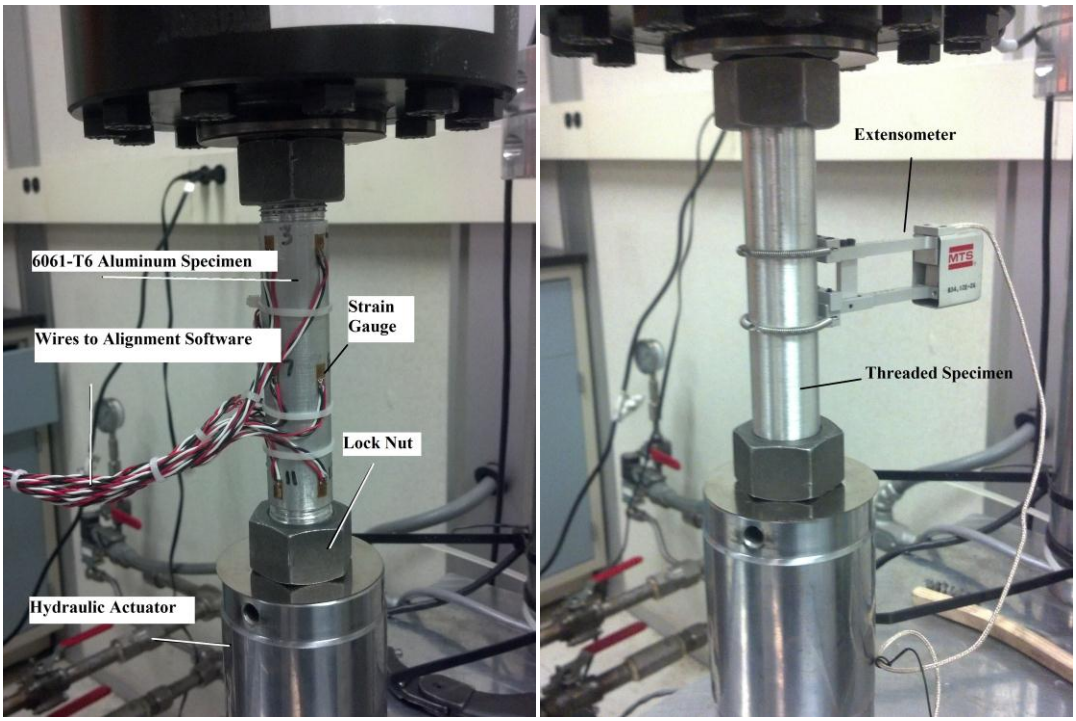

Figure 11: Threaded Aluminum Specimen Alignment Specimen (Right) and Test Setup (Left)

For this strain specimen alignment, the zero load bending was driven as close to zero as possible. The bending strain incurred at load however was determined to be too high (Figure 12). With an alignment thought to be as close as possible, the requisite break-in was accomplished, indicating that the same 500 cycle test configuration would suffice. Then the convergence studies were conducted to maximize the test parameters.

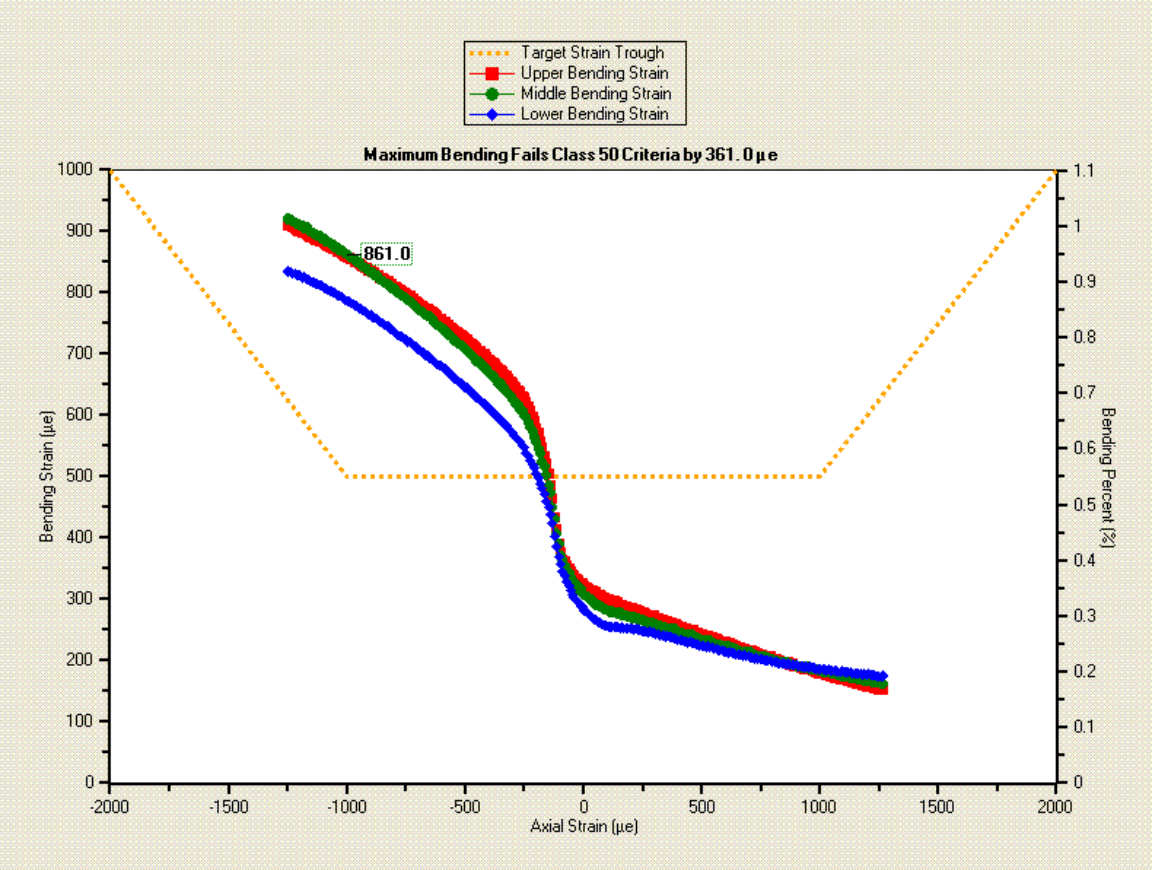

Figure 12: Threaded rod alignment output

With this alignment, Q values peaked at 0.6 Hz cyclic load rate (Q = 282). The low Q seemed to indicate high system damping (perhaps via friction at the actuator from misalignment). It is possible that loosely machined threads on the alignment specimen were allowing some slipping or bending in the specimen. This problem presented itself in the hysteresis loop of another specimen tested later (Figure 13).

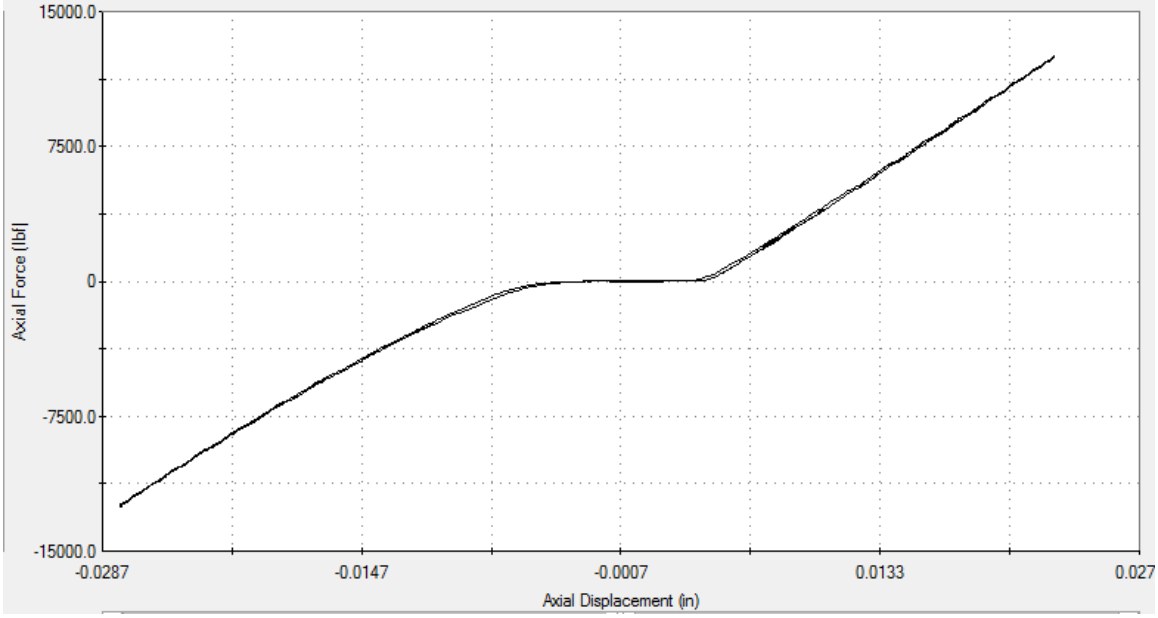

Figure 13: Hysteresis loop skewed by thread slippage

(Note: Indicated force is 12.4% higher than actual force in experimentation)

To fix this alignment problem a mechanical alignment was accomplished using a dial indicator (Figure 14). By fixing the dial indicator to the actuator, then turning the actuator, difference in angle and concentricity of the load cell could be measured and then aligned. After alignment by dial indicator, the ideal cyclic load rate was 1 Hz, and Q = 371. These results were better, but still lower Q values than square bar stock in the V-wedge grips indicated that significant energy dissipation was still occurring in the test system, likely a consequence of more compliance in the load frame due to higher cyclic loads.

Figure 14: Mechanical Alignment of Actuator and Load Cell

Titanium Damping

Though it served well to provide moderate Q values (the highest being Q = 709 in a single 6.35 x 6.35 mm square bar test), aluminum is not a commonly used substrate for hard coatings. The desired end result is to use damping coatings on titanium rotor blades. Furthermore, the round specimens are not favorable to achieve a uniform thickness of sprayed hard coating. Therefore, for comparison to existing damping data and as a flat substrate for hard coating property extraction, the bulk of tests were conducted on Ti-6Al-4V alloy, 6.35 x 12.7 mm rectangular bar stock. Each specimen was 254 mm in

length, 50.8 mm on either side to be gripped, leaving a 152.4 mm working test section. This length was chosen to provide sufficient displacement to reduce the effects instrument inaccuracy. Flat-faced grips were used with alignment stops to keep specimens centered on the load path.

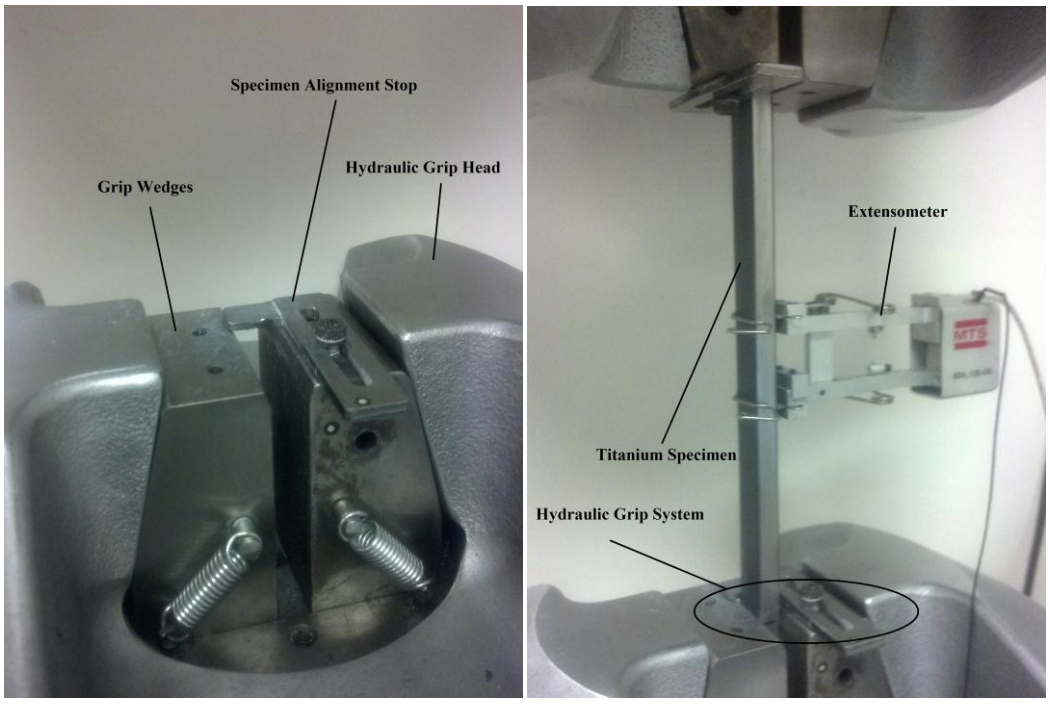

Figure 15: Flat-Faced Wedge Grips (Right) and Titanium Bar Test Setup (Left)

Past work has noted inconsistencies in damping properties between specimens, though to be due to location and orientation of the specimens in the blank material (Easterday 2010)(Pearson 2008). Although all nine titanium specimens tested herein were cut from the same extruded bar stock, the possibility of differing material properties at the bar ends was still of concern. To alleviate this concern, a simple monotonic test was conducted on each specimen to empirically determine the elastic modulus and screen for anomalous properties. The moduli of all specimens fell within less than one percent variation, determined to be acceptable.

After the 4000 cycle break-in, and the monotonic tests, cyclic load amplitudes of 11873 N were used, reaching deformation of approximately 1400 με. The convergence studies were repeated under these conditions, first varying the loading frequency from 0.2 Hz to 3.0 Hz, then the data sample rate from 128 Hz to 1024 Hz. With the test parameters optimized, the bare specimen data was collected at 11873 N fully reversed loads cycled at 1 Hz for 500 cycles. Data was analyzed over the last 300 cycles. Load, displacement, and strain data were sampled at 512 Hz, as determined by convergence study. Each specimen was removed from the grips and refitted for each of ten tests.

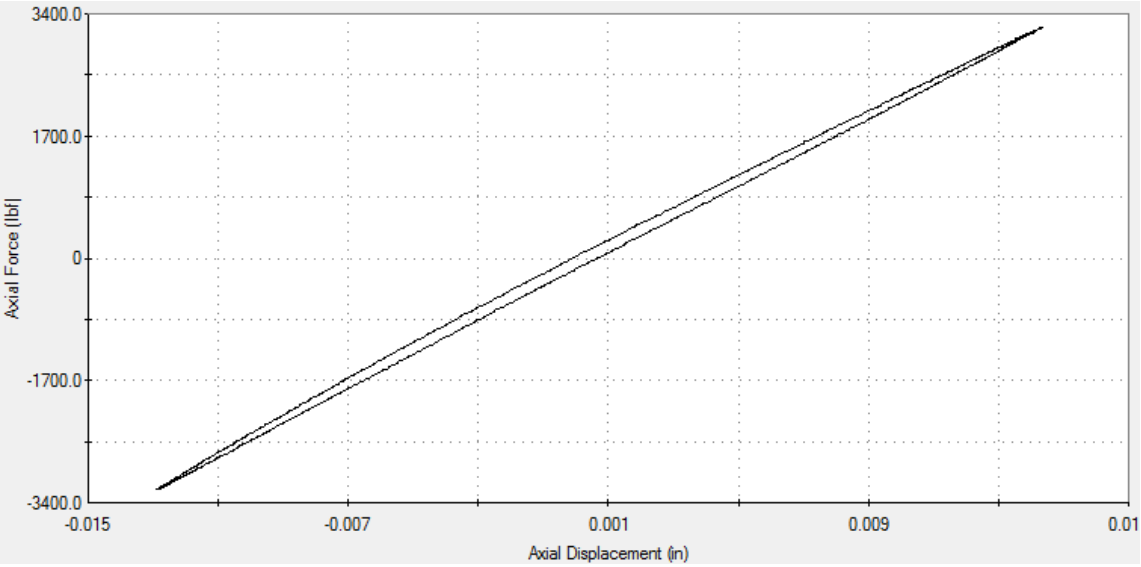

Figure 16: Hysteresis Loop of Titanium Specimen

(Note: Indicated force is 12.4% higher than actual force in experimentation)

The AISI 4140 steel plate had a modulus 1.73 times that of titanium, a cross-sectional area 7.5 times that of the titanium specimens, and a test section 1/2 the length of the titanium specimens. The combination of these factors resulted in 1/26th the displacement measured in the titanium test. The steel plate was then tested under the same parameters as the titanium bars, 1 Hz cyclic load of 11873 N. The resultant

dissipated energy of 0.0172 J was assumed to be attributed to losses at the grip, and could be subtracted from the measured dissipated energy of tests done on titanium.

Coated Titanium Damping

Having documented the dissipated energy of the bare titanium specimens, they were sent to be coated at APS Materials Inc. in Dayton, Ohio. The APS-600 coating was applied only on the 12.7 mm sides of the rectangular specimens. Three different coated lengths were used; 50.8, 101.6, 152.4 mm, all centered on the test section of the specimens. Past tests conducted with bending methods have used partially coated beam lengths. The same approach was applied to determine the best approach to coating property extraction. The coating was applied to an average thickness of 0.295 mm on each side in order to achieve substrate to coating volume ratios equal to those of the data published for this coating.

Figure 17: Coated Titanium Geometry for three specimen types

A monotonic test was conducted to determine the necessary load to achieve 1400 με for comparison to bare substrate results. The resultant parameters, seen in Table 1, were applied to three specimens each.

Table 1: Coating Lengths, Volumes, Volume Ratios, & Test Loads

Coated Length (mm)	**Coating Volume (mm^3)**	**Volume Ratio (Ti/APS-600)**	**Test Load (N) for 1400 με**
50.8	383	32.1	12110
101.6	766	16.05	12347
152.4	1149	10.7	12585

Although the load was increased to keep strain constant, the remaining test parameters were identical to the bare specimen tests. Another 4000 break-in cycles were applied to each specimen at these loads. The fully reversed test load was cycled at 1 Hz and data was sampled at 512 Hz, identical to bare specimen tests. Tests were again 500 cycles in length, the last 300 of which would be analyzed data. With these parameters constant, the knockdown factor of the coating could be determined from the ratio of substrate Q values divided by coated specimen Q values. The results would be compared to previous knock down factor data for the APS-600 coating.

Data Processing

Data files were processed with a few, slightly varied, MATLAB codes. The codes first imported the raw data as output by the MTS controller (a space delineated .dat file format). The 12.4% miscalibration in load data was accounted for by dividing all loads by 1.124 to arrive at the actual load. Then the location of the peak load was found for each cycle. From these peak loads the stored energy of each cycle calculated. The

dissipated energy of each cycle was measured using the "polyarea" function which automates subtraction of two integrals. Finally η and Q were calculated for each cycle, and then the mean and R-STD of these values over 300 cycles were found. Dissipated energy from the grip compliance study was input into the code to be subtracted from raw test results. The resulting outputs, therefore, would be for the specimens only. The Q values for uncoated and coated specimens were divided to determine the coating knockdown factor.

Summary

This chapter examined the experimental setup. Square aluminum bar was used to repeat the results of Scott-Emuakpor et al. Threaded aluminum bar was used to study directly threaded boundary conditions. Titanium provided the bulk of the data in this study, and was then coated to determine coating knockdown factor for comparison to published results. Next, those results will be discussed in more detail.

IV. Results and Discussion

Unreliable Strain Data

One significant problem presented itself immediately. Strain data measurements were observed to be inconsistent, and lead to highly variable energy calculations. This seemed to be a consequence of extensometer slippage. Ideally, stress and strain could be used to directly calculate the Q values of the material only, eliminating consideration of dissipated energy at the grip. Because this data was unreliable, the load and displacement data were used to calculate energy, hence, the need for the grip compliance studies.

Effectiveness of New Controller

The new controller demonstrated vast improvements in the accuracy within each test. The R-STD improved by 40% compared to Scott-Emuakpor et al. Dissipated and stored energies both measured lower, despite identical test parameters, and agreeing MATLAB codes. It was discovered that two of the samples re-tested were not actually used in the original paper by Scott-Emuakpor et al., which would explain the differing average energy measurements. Average results comparison can be seen in Table 2.

Table 2: Comparison of 6.35 x 6.35 mm Aluminum Bar Results

	(Scott-Emuakpor, Runyon and George 2012)	**With Improved Controller Identical Test Parameters**
R-STD (%)	27.35	16.55
Ds (J)	.01432	.00730
Us (J)	.4557	.3654
Q	214	324

Break-In Study

The 4000 preliminary cycles served to identify both boundary condition shifts at the beginning of a test, as well as material break-in period. The quality factor break-in seemed to demonstrate that after 2500 cycles, the material settled into a steady state (Figure 18). This was justified by the steadying of R-STD after a much shorter break-in of 200 cycles (Figure 19), indicating the faster settling of boundary conditions.

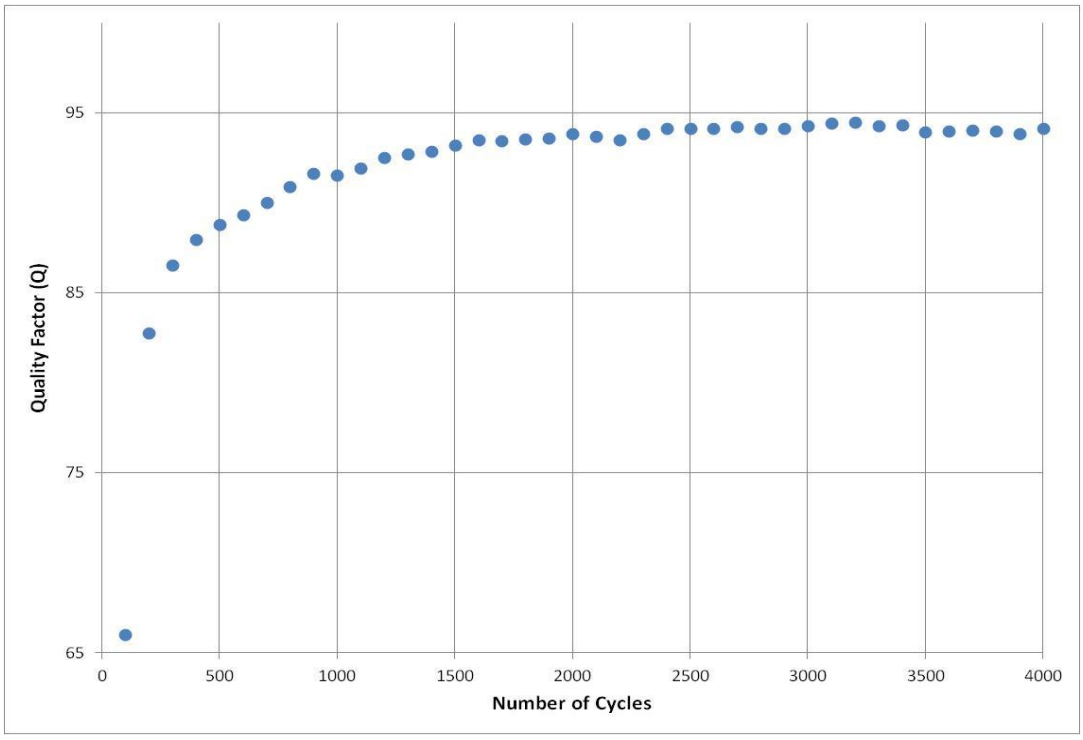

Figure 18: Quality Factor Break-In for Titanium

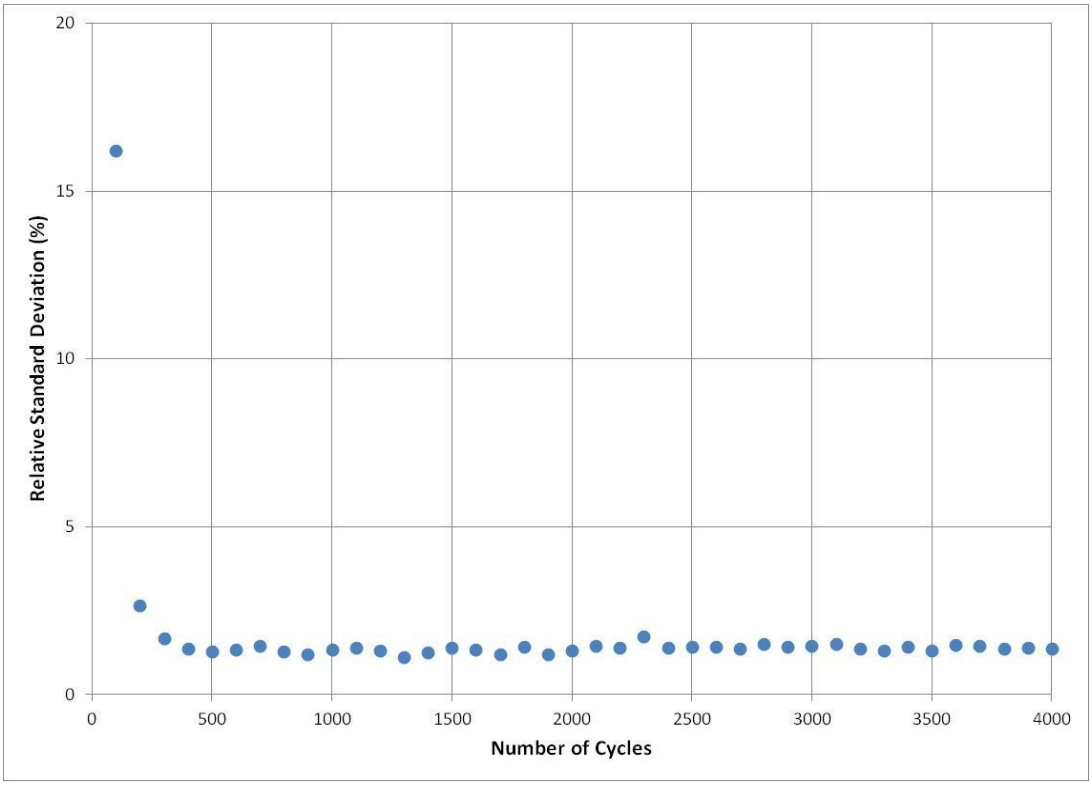

Figure 19: R-STD (per 100 cycle) Break-In for Titanium

Convergence Studies

The convergence studies tended to show the highest Q at 1 Hz cyclic load rate. The only exception to this was in the threaded sample under seemingly inaccurate strain specimen alignment. It seems that a lingering misalignment resulted in additional damping, likely at the actuator seal, which lowered Q values, and shifted the peak frequency. After the mechanical alignment was completed, the threaded sample data matched the rest (Figure 20).

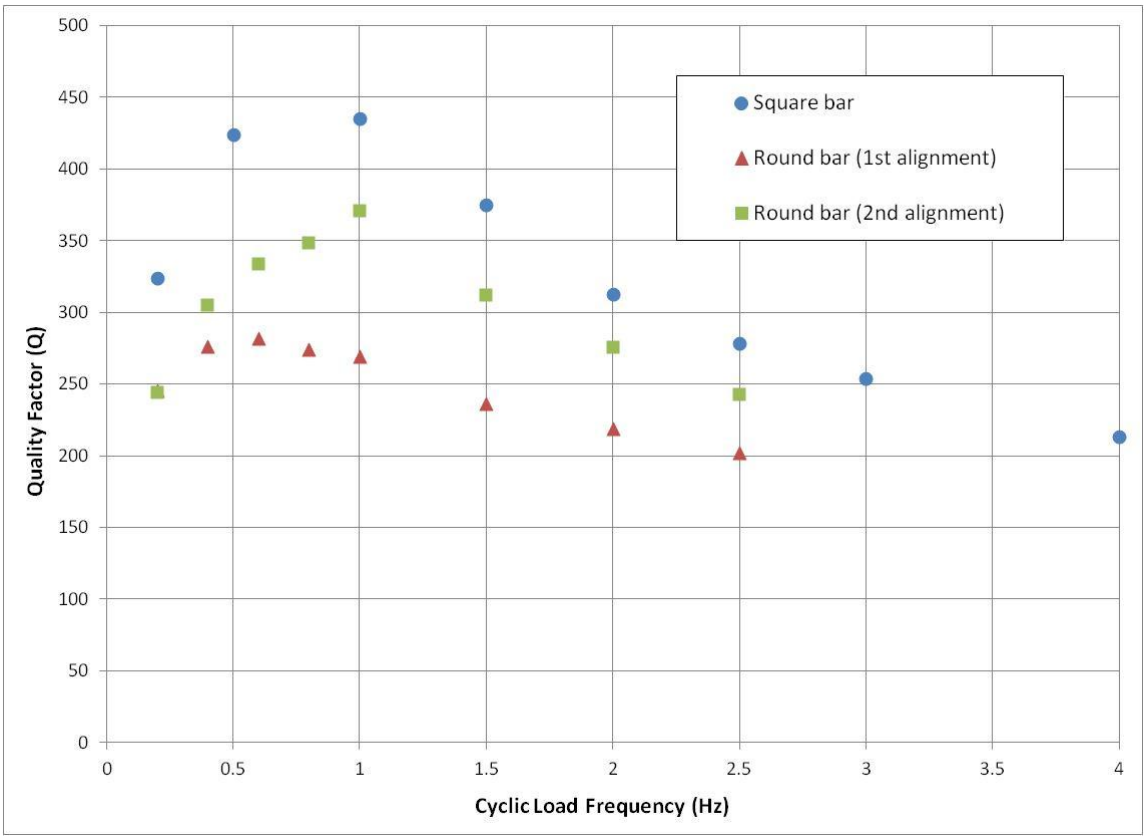

Figure 20: 6061-T6 Cyclic Load Rate vs. Q

In the 6061 Aluminum, the data sample rate had a large impact on R-STD within each test. Higher sample rates resulted in smaller STD but also larger data files, which translates into increased computing time. Above a sample rate of 409 Hz, minimal improvements were made, so this served as the ideal setting for data sample rate (Figure 21). At best, the R-STD for aluminum samples were reduced around 6%, a very acceptable variation for averaging data samples, and a significant improvement from the 16.5% variation as seen with fewer data points.

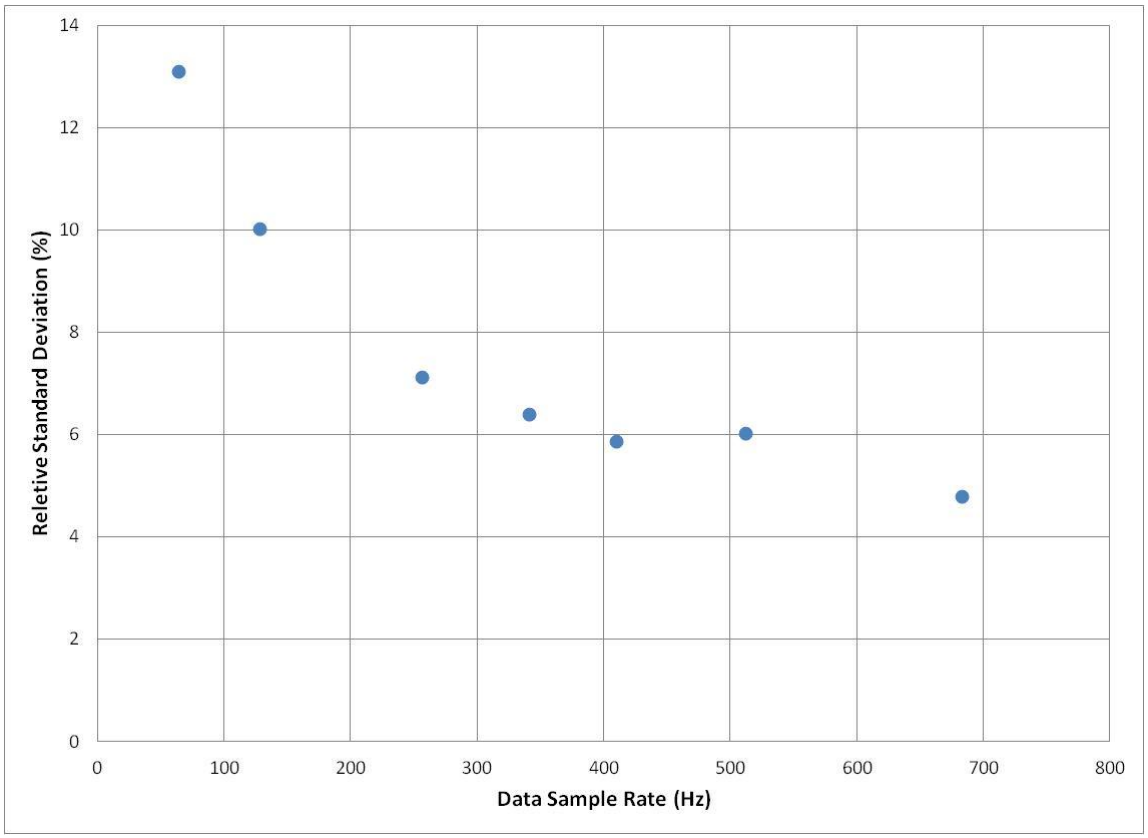

Figure 21: 6061-T6 Data Sample Rate vs R-STD

Convergence in the titanium bars was similar. The highest Q values occurred at cyclic load rates of 1 Hz (Figure 22). The overall Q values were much lower than aluminum however. Titanium is known to have higher inherent damping (Lazan 1968); however, it seems that the higher loads (3X that of aluminum) combined with the flat faced grips resulted in more dissipated energy at the boundary conditions. This drove the grip compliance study as a means to account for losses in the grip mechanism.

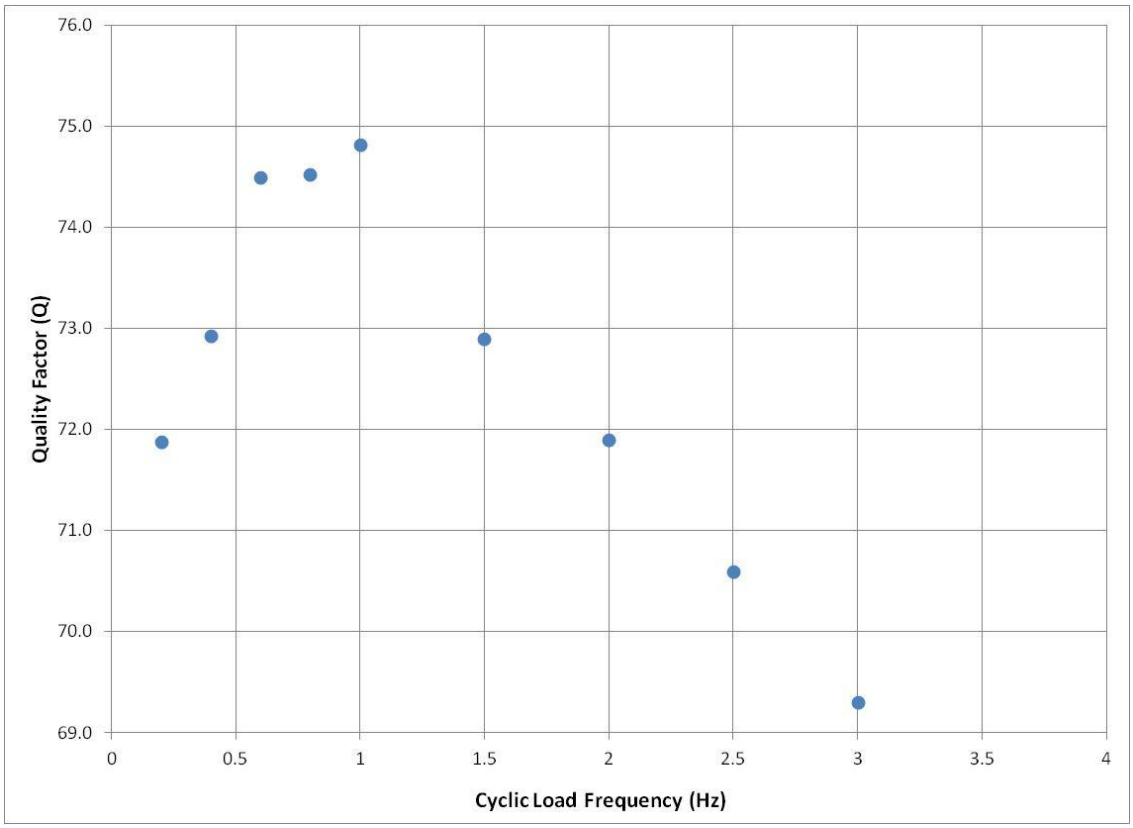

Figure 22: Ti-6Al-4V Cyclic Load Rate vs. Q

Again, the data sample rate convergence for titanium followed a similar trend to that of aluminum. Increased sample rate greatly improved R-STD to a point. Sample rates above a 512 Hz, however, returned minimal gains. The 300 cycle R-STD for titanium was, especially low compared to aluminum, less than 1% in most tests. The larger inherent damping seemed to provide easily measurable dissipated energy.

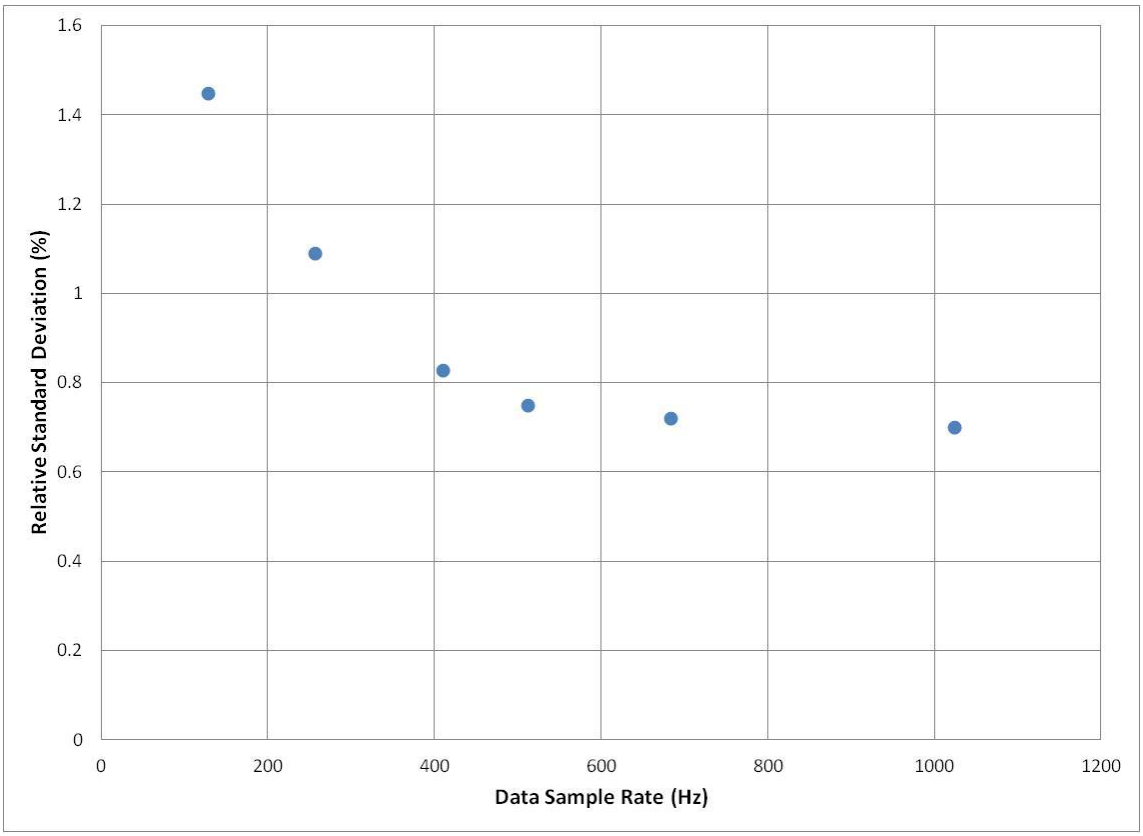

Figure 23: Ti-6Al-4V Data Sample Rate vs. R-STD

Grip Compliance

The study of grip compliance was accomplished to attempt to improve the accuracy of the titanium Q values. Small displacements at the grip resulted in friction and thus, measurable dissipated energy. By subtracting this dissipated energy from the dissipated energy measured in the titanium tests, a more accurate Q value would be established. The average dissipated energy in the compliance test was measured to be 0.0172 J. Once subtracted from the titanium dissipated energy, Q values improved slightly (on the order of 15-20%). This method was used for both coated and uncoated titanium data.

Due to much smaller loads, the compliance for the square aluminum bar test could not be accurately measured, and seemed rather negligible. Though a compliance test for the threaded specimen case could not be designed, the lower quality factor of threaded specimens could be explained by additional compliance brought on by extremely large loads. If this is the case, it would suggest that the best design for a test is a very slender specimen that will only require small loads to deform a measurable amount. This would make the grip and test apparatus appear almost infinitely rigid by comparison, making compliance effects negligible.

Aluminum Characterization

Aluminum convergence data showed peaking Q values at 1 Hz cyclic load rate, and acceptable precision for data sample rates of 409 Hz. Even with these best possible test parameters, the 6061-T6 had some variation between specimens. The Q values varied between specimens, from 358 to 558. The overall repeatability for each specimen was promising (Figure 24). Because 6061-T6 has little in the way of published damping data, a precise numerical comparison could not be made. This alloy is known, however, to have very small damping compared to many other metallic alloys (Lazan 1968). The range of Q values measured in this study still seems lower than expected. Further insight as to possible causes of this will be discussed later. Threaded specimens proved difficult to secure in fixed boundary conditions. Loose thread tolerance may have allowed specimen bending.

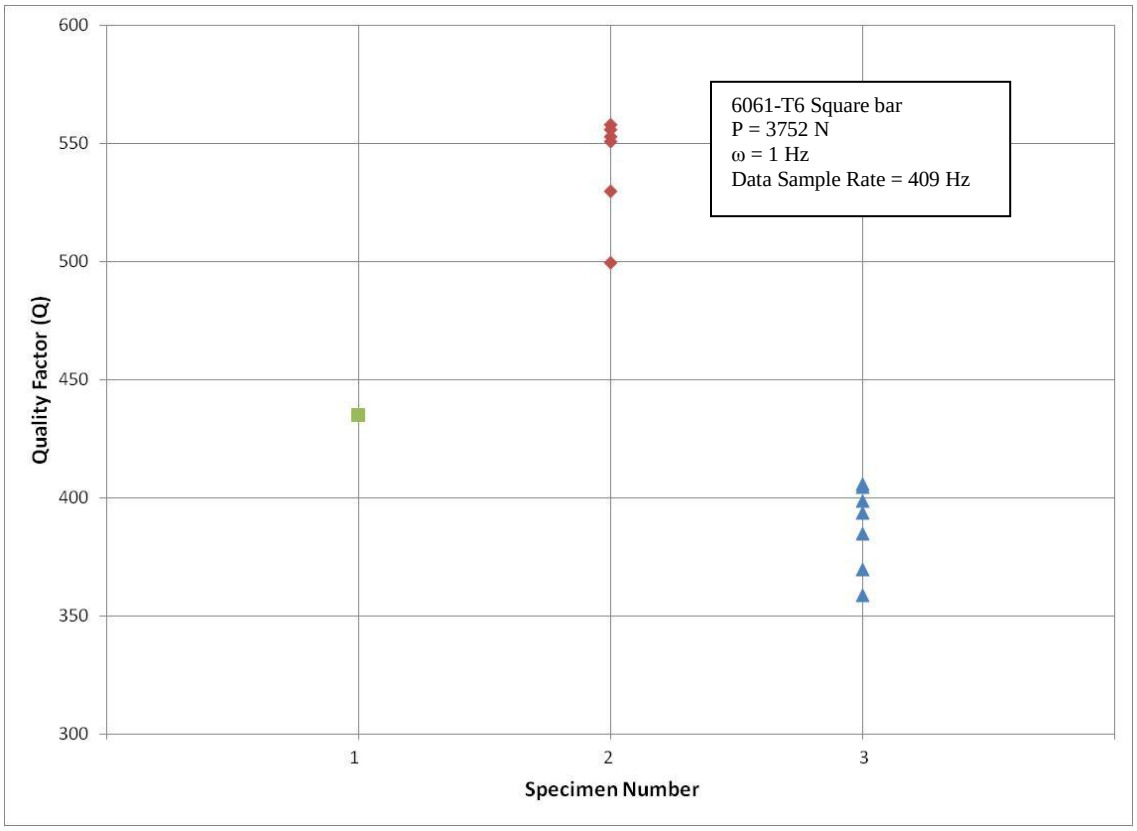

Figure 24: Quality Factor for 6061-T6 Square Bar

Titanium Characterization

Titanium results showed significantly smaller R-STDs within each test (most less than 1%). There was, however more sizeable variation between specimens (Q values ranged from 65 to 113). Although manufacturing inconsistencies were of concern early on, it seems unlikely that they produced the discrepancies. The moduli of all nine titanium specimens were within ±1.33 Msi, or ±0.86%. There was also variation between tests for each specimen. The quickly converging R-STD measurements led to a misjudgment in how many break-in cycles should have been accomplished before useable data was collected. For each titanium specimen, a single test measured noticeably higher Q values. It was realized that for each first test after break-in, the

specimen was not removed, and the boundary conditions were not reset. It seems highly probable that the quality factor break-in *was*, in fact, indicating settling boundary conditions, but on a small enough level so as not to degrade R-STD. If 1500-2000 cycles were run before the collection of usable data, it is likely that the resulting Q values would have been more consistent between tests. The resulting Q values are compiled in Figure 25. Specimens 1, 5, and 7 were coated 50.8 mm, specimens 2, 4, and 8 were coated 101.6 mm, and specimens 3, 6, and 9 were coated over the full 152.4 mm test section. The data is further summarized in

Table 3.

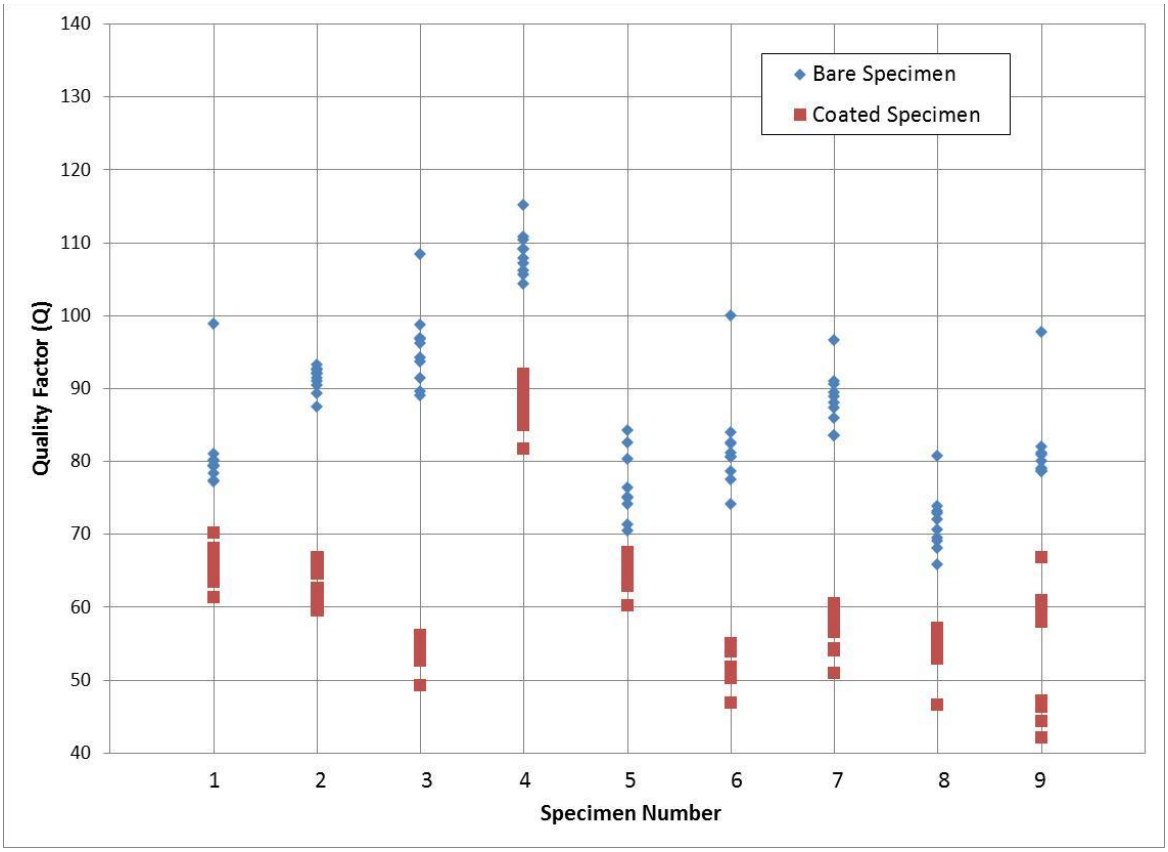

Figure 25: Q Values of Coated and Uncoated Titanium

Table 3: Summary of Coated and Uncoated Titanium Results

Coated Length	Specimen Numbers	Avg. Q (uncoated)	Avg. Q (coated)	Avg. Reduction
50.8 mm	1	81.08	65.90	19%
	5	75.62	64.35	15%
	7	88.47	56.77	36%
	Average	**81.72**	**62.34**	**23%**
101.6 mm	2	91.18	63.17	31%
	4	108.54	88.15	19%
	8	71.56	54.43	24%
	Average	**90.42**	**68.82**	**24%**
152.4 mm	3	95.45	54.01	43%
	6	82.14	57.40	30%
	9	81.78	53.04	35%
	Average	**86.46**	**54.82**	**36%**

The comparison to publish APS-600 data was accomplished considering the aforementioned factor of three between bending and axial analyses.

Table 4: Knockdown factor for APS-600

	Average Q Knockdown	Best Q Knockdown
APS-600 Data (Torvik 2012)	8.95	9.44
Hysteretic Method	1.58	1.77
Hysteretic Bending Equivilent (3x)	4.74	5.30

Summary

The results obtained from the hysteretic energy method have some variability, both between tests, and between specimens. Differences due to coating application were measurable by averages, however, and the knockdown factor measured by hysteretic energy methods (scaled for bending to axial comparison) was within 40% of the results obtained in bending studies conducted on this coating. Some meaningful conclusions can be made from this research.

V. Conclusions and Recommendations

Conclusions of Research

The hysteretic energy method in axial cyclic loading was used to characterize material damping of 6061-T6 aluminum, and both APS-600 coated and uncoated Ti-6Al-4V titanium specimens. Some conclusions can be made following this study.

1. Exploitation of the axial mode of vibration cannot be compared to bending analyses. The quality factor is quite different in this method.
2. Long slender specimens result in larger (more measurable) displacement under small axial loads, which reduce losses due to compliance in the grip.
3. Damping reduction from coatings can be determined, with some variance, by means of averaging many hysteresis loops, over multiple tests.
4. Knockdown factors from the axial method were within 40% of those measured from bending methods.
5. High cycle break-in periods seem to settle any boundary condition slippage and are presumed to result in more consistent results.
6. Higher damping creates more measurable hysteresis loops, and reduces variability within the test measurements.
7. Directly threaded boundary conditions do not necessarily improve quality factor. They will either involve extremely complex manufacturing processes, or they will require very large loads which increase system compliance, producing less accurate Qs.
8. More precise displacement measurements are necessary to produce repeatedly exact and consistent damping determination.
9. Specimen alignment is a critical aspect for achieving the most accurate Q values.

Significance of Research

This research, though with some variance, is the first work to quantify quality factor of titanium in the axial mode. It is also the first to measure Q value knockdown

factor from hard coatings by means of hysteretic energy and compare them to results in bending. The work herein has also provided some meaningful insight into test methodology that should, or should not be used to improve hysteretic damping determination.

Possible Problems

The differences between knockdown factors in bending versus axial methods should be the focus of future research. Optimization of test parameters to achieve the most accurate displacement measurement and lowest system compliance may alleviate this discrepancy. Other possible causes for this difference may be considered. The differing friction between steel and titanium may have caused inaccurate measurement of compliance energy. It is possible that the comparison between bending and axial tests is more complex due to differing microstructure interaction. This could be determined by conducting a hysteretic energy test in three-point bending to establish a bending knockdown factor via the hysteretic energy method.

Future Research

The findings of this study point in a particular direction, and future research will seek to optimize this test method with the following approaches.

1. Design test specimens to be very slender so as to displace under smaller loads.
2. Design the length of the specimen to be long enough to produce large displacements at the desired strain, without risk of buckling.
3. Utilize a high number of cycles to break in the boundary conditions before measuring the useful data cycles.

4. Increase frequency resolution in convergence studies to better maximize resultant quality factor.
5. Investigate more precise displacement measurement methods, i.e. extensometer to improve precision.
6. Extend best methods into environmental modification, and R > -1 stress ratios.

Summary

The hysteretic energy method of damping determination is nearing usefulness. A few more small advancements in methodology and precision will make damping determination significantly easier than current bending methods and will open damping testing to precise environmental and stress ratio variation.

Appendix A: Representative MATLAB Code

```
% CAPTAIN COLIN ENGEBRETSEN, AFIT/ENY 2012
% HYSTERETIC ENERGY DAMPING METHOD
% .dat file, 500 cycles (beginning in row 8), 200 break-in, 300 data
% | disp (in) | force (lbf) | microstrain | Stress (psi) | time (s) |
close all
clear all
clc
format shortG

A=1/8;
L=6;
V=L*A;

clc
%
% GUI FILE FINDER
[filenames,path]=uigetfile('.dat','multiselect','on');
Tot=0;

% Loop executed for each file selected
for loop=1:length(filenames)

  if ischar(filenames)==1
  filename=[path,filenames];
  else
  filename=[path,filenames{loop}];
  end

  % RAW DATA READ-IN & CONCATENATION
  rawdata=dlmread(filename, ' ', 8, 0);

  % MANIPULATION TO REMOVE STARTUP FLUX
  dat1=round(rawdata(:,2)/100);
  first=find(dat1,1)-1;
  force=rawdata(abs(rawdata(1:first,2))==min(abs(rawdata(1: first,2))),2);
  dis=rawdata(abs(rawdata(1:first,2))==min(abs(rawdata(1: first,2))),1);
  rawdata=[rawdata(first : end,1)-dis rawdata(first : end,2:3)...
  rawdata(first : end,2)/A rawdata(first : end,4)];
  clear dat first
  rawdata(:,2)=rawdata(:,2)/1.124; % Accounting for load cell calibration error

  % Check for extra spaces in data
  if length(find(rawdata==0))>1
  disp('POSSIBLE ERROR IN DATA.  REMOVE BACK-TO-BACK SPACES')
  disp(filename)
  if ischar(filenames)==1
  return
  else
  continue
  end
  end

  % DETERMINING CYCLE PEAK INDICES
  dat=rawdata(:,2);
  tops=[];
  for x=9:length(dat)-9
  if dat(x)>0
```

```
  if dat(x)>dat(x+1) && dat(x)>=dat(x-1) && dat(x)>dat(x-2) &&
dat(x)>=dat(x+2)...
  && dat(x)>=dat(x-3) && dat(x)>dat(x+3) && dat(x)>dat(x-4) &&
dat(x)>=dat(x+4)...
  && dat(x)>=dat(x-5) && dat(x)>dat(x+5) && dat(x)>dat(x-6) &&
dat(x)>=dat(x+6)...
  && dat(x)>=dat(x-7) && dat(x)>dat(x+7) && dat(x)>dat(x-8) && dat(x)>=dat(x+8)
  tops=[tops;x];
  end
  end
  end
  clear dat x
  % Ensure that resulting data counts 500 cycles
  if isequal(length(tops),500)==0
  disp('ERROR IN DATA FILE: NOT 500 CYCLES');
  disp(filename)
  continue
  end
  % Make sure that a single peak is indexed for each loop
  for id=2:length(tops)
  diffs=tops(id)-tops(id-1);
  if isempty(find(diffs<(mean(diffs)-4)))==0
  disp('ERROR: DOUBLE TOPPING');
  disp(filename)
  continue
  end
  end
  % Parameters denoting how many loops to ignore and percentage to be
  % truncated if sine taper was used at the end of the test
  N=round((length(tops))*1);
  skip=200;
  tops=tops(skip:N);

  % SEGREGATE LOOPS; MEASURE AREA: CALCULATE LOSS & Q
  DS=zeros(N-skip,1);
  US=zeros(N-skip,1);
  DS2=zeros(N-skip,1);
  US2=zeros(N-skip,1);
  loss=zeros(N-skip,1);
  Q=zeros(N-skip,1);
  for x=1:N-skip
  DS(x,1)=polyarea([rawdata(tops(x):tops(x+1),1);rawdata(tops(x),1)],...
  [rawdata(tops(x):tops(x+1),2);rawdata(tops(x),2)]);
  US(x,1)=0.5*rawdata(tops(x),1)*rawdata(tops(x),2);

DS2(x,1)=polyarea([rawdata(tops(x):tops(x+1),3);rawdata(tops(x),3)]*(L/1000000)
,...
  [rawdata(tops(x):tops(x+1),2);rawdata(tops(x),2)]);
  US2(x,1)=0.5*rawdata(tops(x),3)*rawdata(tops(x),2)*(L/1000000);
  loss2(x,1)=DS2(x,1)/(2*pi*US2(x,1));
  loss(x,1)=DS(x,1)/(2*pi*US(x,1));
  Q(x,1)=1/loss(x,1);
  Q2(x,1)=1/loss2(x,1);
  end

  % Ensures again that all measured loops are valid
  if isempty(find(DS==0))==0
  disp('POSSIBLE ERROR IN DATA.  ZERO CYCLE PROBLEM')
  disp(filename)
  continue
  end
```

```
  if isempty(find(US==0))==0
  disp('POSSIBLE ERROR IN DATA.  ZERO CYCLE PROBLEM')
  disp(filename)
  continue
  end
  % Compilation of data for output
  MDS=mean(DS);
  MUS=mean(US);
  ML=mean(loss);
  MQ=mean(Q);
  Tot(loop)=MDS;
  SDS=std(DS);
  SUS=std(US);
  SL=std(loss);
  SQ=std(Q);
  RDS=std(DS)/mean(DS)*100;
  RUS=std(US)/mean(US)*100;
  RL=std(loss)/mean(loss)*100;
  RQ=std(Q)/mean(Q)*100;
  stats={' ' 'DS (in-lb)' 'US (in-lb)' 'Loss factor' 'Quality factor';...
  'Mean' MDS MUS ML MQ; 'STD' SDS SUS SL SQ; 'R-STD (%)' RDS RUS RL RQ};
  if ischar(filenames)==1
  stats{1,1}=filenames
  return
  end
  stats{1,1}=filenames{loop}

  % The following is stress strain calculations of loss and Q
  % they were usually found to be extremely inacurate

%
%  STATS2=cell(4,5);
%  MDS2=mean(DS2);
%  MUS2=mean(US2);
%  ML2=mean(loss2);
%  MQ2=mean(Q2);
%  SDS2=std(DS2);
%  SUS2=std(US2);
%  SL2=std(loss2);
%  SQ2=std(Q2);
%  RDS2=std(DS2)/mean(DS2)*100;
%  RUS2=std(US2)/mean(US2)*100;
%  RL2=std(loss2)/mean(loss2)*100;
%  RQ2=std(Q2)/mean(Q2)*100;
%  STATS2={' ' 'DS (in-lb)' 'US (in-lb)' 'Loss factor' 'Quality factor';...
%  'Mean' MDS2 MUS2 ML2 MQ2; 'STD' SDS2 SUS2 SL2 SQ2; 'R-STD (%)' RDS2 RUS2 RL2
RQ2};
%
%  if ischar(filenames)==1
%  STATS2{1,1}=filenames
%  return
%  end
%  STATS2{1,1}=filenames{loop}
end
```

Bibliography

Blackwell, Christopher M. *The Evaluation of the Damping Characteristics of a Hard Coating on Titanium.* Air Force Institute of Technology (AU), Wright-Patterson AFB OH, 2004.

Easterday, Oliver T. *An Experimental Characterization of Damping Properties of Thermal Barrier Coatings at Elevated Temperatures.* Air Force Institute of Technology (AU), Wright-Patterson AFB OH, 2010.

Flügge, Wilhelm. *Viscoelasticity.* 2nd Ed. New York: Springer-Verlag, 1975.

Henderson, John P., Ahid D. Nashif, J. E. Hansel, and R. M. Wilson. "Enhancing the Passive Damping of Plasma Sprayed Ceramic Coatings." *Advanced Ceramic Coatings and Interfaces IV* 30, no. 3 (2009).

Indian Institute of Technology Roorkee. "Noise and Vibration Control Damping." *Indian Institute of Technology Roorkee.* http://www.iitr.ac.in/outreach/web/CIRCIS/UG/NVC/2%20Damping.pdf.

Instron Corporation. "7 Tips for Materials Testing." Norwood, MA, 2006.

Ivancic, Frank T. *The Effect of a Hard Coating on the Damping and Fatigue Life of Titanium.* Air Force Institute of Technology (AU), Wright-Patterson AFB OH, 2003.

Lazan, Benjamin J. *Damping of Materials and Members in Structural Mechanics.* New York: Pergamon Press, 1968.

Limarga, A. M., T. L. Duong, G. Gregori, and D. R. Clarke. "High-Temperature Vibration Damping of Thermal Barrier Coating Materials." *Surface & Coatings Technology* 202, no. (4-7) (2007): 693-697.

Meirovitch, Leonard. *Fundamentals of Vibrations.* New York: McGraw-Hill, 2001.

Nashif, Ahid D., David I. G. Jones, and John P. Henderson. *Vibration Damping.* New York: John Wiley & Sons, 1985.

Nicholas, Theodore. *High Cycle Fatigue; A Mechanics of Materials Perspective.* San Diego: Elsevier inc., 2006.

Patsias, S., A. Byrne, and M. Shipton. “Hard Damping Coatings: Optimization of Damping Effectiveness by Controlling the Deposition Parameters.” *9th National Turbine Engine High Cycle Fatigue Conference*, 2004.

Patsias, S., N. Tassini, and K. Lambrinou. “Ceramic coatings: Effect of deposition method on damping and modulus of elasticity for yttria-stabilized zirconia.” *Materials Science and Engineering*, no. 442 (2006): 504 - 508.

Pearson, Lindell E. *Vibration Analysis of Commercial Thermal Barrier Coatings.* MS thesis, AFIT/GAE/ENY/08-J05. School of Engineering and Management, Air Force Institute of Technology (AU), Wright-Patterson AFB OH, 2008.

Reed, Shad A. *Development of Experimental, Analytical, and Numerical Approximations Appropriate for Nonlinear Damping Coatings.* Air Force Institute of Technology (AU), Wright-Patterson AFB OH, 2007.

Scott-Emuakpor, Onome E., Brian D. Runyon, and Tommy J. George. “A Hysteretic Energy Method for Determining Damping Properties of Hard Coatings.” 53rd AIAA/ASME/ASCE/AHS/ASC Structures, Structural Dynamics and Materials Conference Report, 2012.

Tassini, N., S. Patsias, and K. Lambrinou. “Ceramic coatings: A phenomenological modeling for damping behavior related to microstructural features.” *Materials Science and Engineering*, no. 442 (2006): 509 - 513.

Torvik, Peter J. “Determining Damping from the Hysteresis Loop Area.” Unpublished Report, Xenia, OH, 2013.

Torvik, Peter J. “Material Properties of APS COATING 1.” Report to APS Materials Inc., Dayton OH, August, 2012.

Torvik, Peter J. “On the Determination of the Damping Properties of Coatings.” Unpublished Report, Xenia, OH, 2011.

Torvik, Peter J., S. Patsias, and G. R. Tomlinson. “Characterising the Damping Behaviour of Hard Coatings: Comparisons from Two Methodologies.” *7th National Turbine Engine High Cycle Fatigue Conference Proceedings*, 2002.

Vaidya, R. U., A. K. Zurek, D. A. Wolfenden, D. A. Bowles, and M. W. Cantu. “Effect of Plasma-Sprayed Alumina on the Strength, Elastic Modulus, and Damping of Ti-25Al-10Nb-3V-1Mo Intermetallic.” *Journal of Materials Engineering and Performance* 4, no. 3 (1995): 252-258.

Van, Ky Dang, and Ioannis Vassileiou Papadopoulos. *High-Cycle Metal Fatigue; From Theory to Applications.* New York: Springer-Verlag Wien, 1999.

Younossi, Obaid, Mark V. Arena, Richard M. Moore, Mark Lorell, Joanna Mason, and Jogn C. Graser. *Military Jet Engine Acquisition.* Santa Monica: RAND, 2002.

REPORT DOCUMENTATION PAGE

Form Approved
OMB No. 074-0188

PLEASE DO NOT RETURN YOUR FORM TO THE ABOVE ADDRESS.

1. REPORT DATE *(DD-MM-YYYY)*	2. REPORT TYPE	3. DATES COVERED *(From – To)*
21-03-2013	Master's Thesis	Oct 2012 – Mar 2013

4. TITLE AND SUBTITLE
Using Hysteretic Energy to Evaluate Damping Characteristics of Hard Coating on Titanium

5a. CONTRACT NUMBER

5b. GRANT NUMBER

5c. PROGRAM ELEMENT NUMBER

6. AUTHOR(S)
Engebretsen, Colin C., Captain, USAF

5d. PROJECT NUMBER

5e. TASK NUMBER

5f. WORK UNIT NUMBER

7. PERFORMING ORGANIZATION NAMES(S) AND ADDRESS(S)
Air Force Institute of Technology
Graduate School of Engineering and Management (AFIT/EN)
2950 Hobson Way, Building 640
WPAFB OH 45433

8. PERFORMING ORGANIZATION REPORT NUMBER
AFIT-ENY-13-M-13

9. SPONSORING/MONITORING AGENCY NAME(S) AND ADDRESS(ES)
AFRL-Turbine Engine Fatigue Facility
Dr. Onome Scott-Emuakpor, AFRL/RQTI
Building 252 Room 20
Wright-Patterson Air Force Base, Dayton, OH 45433-7251
Telephone: (937)-785-6810, Email: onome.scott-emuakpor@wpafb.af.mil

10. SPONSOR/MONITOR'S ACRONYM(S)
AFRL/RQTI

11. SPONSOR/MONITOR'S REPORT NUMBER(S)

12. DISTRIBUTION/AVAILABILITY STATEMENT
APPROVED FOR PUBLIC RELEASE; DISTRIBUTION UNLIMITED

13. SUPPLEMENTARY NOTES
This material is declared a work of the U.S. Government and is not subject to copyright protection in the United States.

14. ABSTRACT

Current methods of material damping evaluation consist of bending tests involving half-power bandwidth base excitation or free decay methods measured by laser vibrometer. These methods are accompanied by complex, nonlinear strain evaluation; they are vulnerable to undesired air damping; and they require less than commonplace equipment. The measurement of hysteretic energy loss in axial cyclic loading alleviates these difficulties. By using common tensile testing machines, strain is kept linear and air damping is of no concern. Furthermore, the static test section allows for simplified environmental variation for high temperature or high humidity testing. This study set forth to advance and refine the hysteretic energy method for determining material damping properties. Convergence studies were conducted to determine test parameters which produced the most accurate results. Bare titanium bars were tested to compare damping values to current measurement techniques. Boundary conditions were studied to determine the effects of losses for different grip mechanisms. Hard coatings were applied to titanium and tested to determine the feasibility of extracting coating properties using this method.

15. SUBJECT TERMS
Hysteresis, Damping, Titanium, APS, APS-600, Fatigue, Hard coating

16. SECURITY CLASSIFICATION OF:			17. LIMITATION OF ABSTRACT	18. NUMBER OF PAGES	19a. NAME OF RESPONSIBLE PERSON
a. REPORT	b. ABSTRACT	c. THIS PAGE			Dr. Anthony Palazotto (ENY)
U	U	U	UU	74	19b. TELEPHONE NUMBER *(Include area code)* (937) 255-3636, x 4599 (Anthony.palazotto@afit.edu)